Available online at www.sciencedirect.com
SCIENCE DIRECT®
Journal of Computational Physics 209 (2005) 249–289
JOURNAL OF COMPUTATIONAL PHYSICS
www.elsevier.com/locate/jcp

Residual distribution for general time-dependent conservation laws

Mario Ricchiuto [a,*], Árpád Csík [b], Herman Deconinck [a]

[a] *von Karman Institute for Fluid Dynamics, Department of Aeronautics and Aerospace, 72 Chaussée de Waterloo, B-1640 Rhode-Saint-Genèse, Belgium*
[b] *Katholieke Universiteit Leuven, Department of Mathematics, Center for Plasma-Astrophysics, Leuven Celestijnenlaan 200B, B3000 Belgium*

Received 15 December 2004; received in revised form 21 February 2005; accepted 1 March 2005
Available online 23 May 2005

Abstract

We consider the second-order accurate numerical solution of general time-dependent hyperbolic conservation laws over unstructured grids in the framework of the Residual Distribution method. In order to achieve full conservation of the linear, monotone and first-order space–time schemes of (Csík et al., 2003) and (Abgrall et al., 2000), we extend the conservative residual distribution ($\mathscr{CRD}$) formulation of (Csík et al., 2002) to prismatic space–time elements. We then study the design of second-order accurate and monotone schemes via the nonlinear mapping of the local residuals of linear monotone schemes. We derive sufficient and necessary conditions for the well-posedness of the mapping. We prove that the schemes obtained with the $\mathscr{CRD}$ formulation satisfy these conditions by construction. Thus the nonlinear schemes proposed in this paper are always well defined. The performance of the linear and nonlinear schemes are evaluated on a series of test problems involving the solution of the Euler equations and of a two-phase flow model. We consider the resolution of strong shocks and complex interacting flow structures. The results demonstrate the robustness, accuracy and non-oscillatory character of the proposed schemes.

Keywords: Unstructured grids; Time-dependent problems; Residual distribution; Conservation; Space–time methods; Monotone shock capturing; High-order schemes

1. Introduction

In this paper we propose high-order schemes for the discretization of systems of conservation laws lacking a multidimensional conservative linearization [1]. Our primary interest is the approximation of

* Corresponding author.
E-mail addresses: ricchiut@vki.ac.be (M. Ricchiuto), arpi@vki.ac.be (Á. Csík), deconinck@vki.ac.be (H. Deconinck).

0021-9991/$ - see front matter © 2005 Elsevier Inc. All rights reserved.
doi:10.1016/j.jcp.2005.03.003

time-dependent solutions containing strong interacting discontinuities. The development of robust high-order schemes is a widespread research topic in the CFD community. Even if Finite Volume ($\mathscr{FV}$) and Finite Element ($\mathscr{FE}$) methods are routinely used for fluid flow simulations, a margin for improvement is still present especially with respect to accuracy and robustness on unstructured meshes. This justifies the study of alternative techniques. Here, we consider schemes of the *Residual Distribution* ($\mathscr{RD}$) or *Fluctuation Splitting* ($\mathscr{FS}$) class, emerged in the last decades as an alternative to the $\mathscr{FV}$ and $\mathscr{FE}$ approaches [2–8]. The interest in $\mathscr{RD}$ stems from the possibility of combining the compactness of the stencil typical of continuous $\mathscr{FE}$ methods with shock capturing capabilities which, as in $\mathscr{FV}$ schemes, do not require the addition of nonlinear dissipative operators to the discretization. Moreover, the schemes operate on arbitrary unstructured meshes. The application of $\mathscr{RD}$ to the solution of the steady Euler and Navier–Stokes equations has already shown a great potential [2–15].

Some issues are however still to be solved to allow the use of $\mathscr{RD}$ to approximate *weak solutions of time-dependent systems* of practical interest such as the Euler equations for gases in thermochemical equilibrium or with more complex forms of thermodynamics, the MHD equations, two-phase flow models and the shallow-water equations, to cite some. Among these issues, the most relevant are, in our view, an efficient stable and accurate extension of the method to the time-dependent case, a conservative formulation allowing to handle general forms of thermodynamics, and the development of a well-understood procedure for the systematic construction of nonlinear high-order schemes yielding a stable and non-oscillatory approximation of discontinuities. An overview of these issues is given in the following subsections.

1.1. Residual distribution for time-dependent problems

The use of $\mathscr{RD}$ for time-dependent simulations has seen a very strong progress in the last years and it is still a very intense research topic. The main focus of the research is the construction of a framework within which is possible to design discretizations retaining the residual character of the steady schemes, as well as to design linear first-order schemes with stable and non-oscillatory shock capturing properties to be used as a basis for the construction of nonlinear high-order schemes. It has been always known that in their basic formulation $\mathscr{RD}$ schemes cannot be more than first-order accurate in time-dependent computations, due to an inconsistent spatial discretization. Early attempts to cure this problem have resorted to a *Petrov–Galerkin* ($\mathscr{PG}$) $\mathscr{FE}$ formulation of the schemes leading to the introduction of a Finite Elements *mass-matrix* [16,17]. This approach has been shown to be very effective in the construction of linear second-order schemes but it leaves open the issue of the construction of non-oscillatory discretizations, since the $\mathscr{PG}$ analogy does not apply to linear positive $\mathscr{RD}$ schemes. Similarly, in [18–23] Caraeni and his collaborators have presented schemes in which the time-derivative is consistently included in the definition of the residual. The authors are able to construct in this way second-order schemes for time-dependent calculations. They have also proposed an extension of their approach allowing to achieve third order of accuracy on structured meshes. As in the case of the $\mathscr{PG}$ formulation, this technique does not generalize to linear positive schemes and hence it does not allow to construct non-oscillatory approximations of discontinuous solutions. Both the $\mathscr{PG}$ schemes and the schemes of Caraeni can be shown to belong to a general family of discretizations making use of a $\mathscr{FE}$-like mass-matrix consistent with the spatial discretization [24]. Two more approaches can be found in the literature to apply $\mathscr{RD}$ schemes for unsteady simulations. The first relies on the use of the residual distribution formulation of the Lax–Wendroff (LW) scheme [2,25–27]. Indeed, this scheme can be shown to be second order in space and time on structured triangulations [27]. However, this property has not been proved or verified on truly unstructured meshes on which most probably also the LW scheme needs the introduction of properly constructed mass-matrix. Moreover, also in this case, the issue of the construction of non-oscillatory schemes remains open. The study of consistent $\mathscr{RD}$ discretizations of time-dependent problems has led at last to the *space–time* formulation of the schemes. Two different, though similar in spirit, research lines have appeared in the literature. One is due to the work reported

in [28–30] in which the authors have written the solution of the time-dependent problem as a sequence of steady problems on space–time *slabs* discretized with space–time linear elements (triangles for 1D problems and tetrahedra for 2D problems). The use of *standard* $\mathscr{RD}$ schemes in each space–time slab, allows to obtain discretizations retaining *all* the properties of the steady schemes. The *time-marching* character of the procedure is guaranteed by the use of upwind $\mathscr{RD}$ schemes and by the satisfaction of a time-step constraint. In the references, however, the authors propose a *double-layer* formulation in which, by solving at once for the values of the unknown in two successive time levels, *unconditionally* monotone and stable linear schemes can be designed. Although this approach allows to construct schemes with all the desired properties and to immediately use all the *numerical artillery* developed for the steady case, it has the drawback of being inherently complex and expensive due to the introduction of time as an additional *independent* unknown, to the generation and storage of the space–time mesh, and to the need of solving for a number of unknowns larger than the number of nodes in the spatial grid, even in its *single-layer* formulation. A space–time formulation of residual distribution making use of *prismatic* space–time elements has been instead proposed in [31–33]. In the references, the authors design both linear second-order and linear positive $\mathscr{RD}$ schemes for time-dependent problems. As before, the space–time formulation allows to reuse all the numerical tools developed for steady simulations. Moreover, the use of prismatic elements guarantees that the number of unknowns is, in the basic formulation of the method, equal to the number of nodes in the grid. At steady-state the schemes of [31–33] reduce to known $\mathscr{RD}$ discretizations. However, the linear first-order positive schemes they propose are constrained by a time-step limitation. Using a double layer formulation similar to the one introduced in [28–30], this limitation has been overcome in [32–34] where unconditionally monotone and stable linear first-order schemes have been proposed. Note that the extension of the space–time schemes of [28–30] to prismatic space–time meshes has been reported in [35]. The framework proposed in [32–34] and [35] is at the moment the only one allowing to design schemes retain all the properties of steady $\mathscr{RD}$. In particular it allows to make use of the tools developed for steady calculations and to construct linear and nonlinear non-oscillatory schemes in a natural and consistent way.

1.2. Conservative formulations of residual distribution

The issue of finding a general conservative formulation of residual distribution, stems from the fact that the computation of discontinuous solutions free of numerical oscillations heavily relies on the use of the first-order N scheme [12,36,37]. The problem is that this scheme makes extensive use of the *non-conservative* quasi-linear form of the equations and cannot be conservative unless a multidimensional Roe linearization is used for the flux Jacobians. Unfortunately, this linearization is only available on simplicial elements and in the case of computations of flows of gases with simple thermodynamics [1]. This has limited the application of $\mathscr{RD}$ mainly to the computation of flows of perfect gases on triangular (in 2D) and tetrahedral (in 3D) meshes.

The first attempts to solve this issue have been based on ad hoc corrections of a non-conservative formulation of the scheme [38,39]. In the references, conservation is achieved by adding to the discrete equations terms dependent on the *discrete conservation error*, thus correcting the non-conservative nature of the scheme. However, the way in which these corrections have to be included into the discretization is somewhat arbitrary. A more consistent framework for the construction of conservative variants of the N scheme has been proposed in [40]. In the reference, the authors propose a class of non-conservative discretizations based on Gauss volume integration of the quasi-linear form in entropy variables. Using the properties of the Gaussian integration, they are able to prove that their schemes indeed converge to the correct weak-solutions of the differential problem. They show how to use their approach to design an N scheme based on the adaptive quadrature of the quasi-linear form of the Euler equations in symmetrizing variables. This technique can be extended to any system of conservation laws with a convex entropy extension, thus solving the problem of the application of $\mathscr{RD}$ in absence of

a conservative linearization. The approach of [40] is based on sound mathematical arguments. Global entropy stability on fine meshes can be shown for the N scheme proposed in the reference, while its L_∞ stability can be shown using a wave decomposition technique [41–43]. The numerical results confirm the theoretical analysis performed in the paper. However, this technique has the drawback of being quite expensive since the number of quadrature points needed to achieve a correct approximation of shocks can be large. A simpler, yet effective, technique has been proposed in [44]. The idea is to approximate directly the integral form of the equations to define the residual. In this way discrete conservation is always guaranteed, provided that a *consistency* constraint is respected. The authors have introduced the terminology $\mathscr{CRD}$ to denote their schemes, indicating that conservation is guaranteed by the definition of the residual as the contour integral of the fluxes on the boundary of the elements of the grid as opposed to the $\mathscr{LRD}$ schemes for which conservation is guaranteed by the conservative linearization. In the paper it is shown how to construct a conservative variant of the N scheme which does not need a Roe linearization. When applied to the Euler equations, this $\mathscr{CRD}$ N scheme shows performances identical to the $\mathscr{LRD}$ N scheme of [12]. Compared to the N scheme based on adaptive quadrature of [40], the $\mathscr{CRD}$ N scheme is more efficient and computationally cheaper due to the fact that a few Gaussian points are needed on each edge of the grid elements while the flux Jacobians are evaluated in a single state. No particular theoretical properties have however been proved for the $\mathscr{CRD}$ N scheme. The application of this technique to the solution of the ideal MHD equations is shown in [44], while its use to construct $\mathscr{RD}$ schemes on meshes composed of quadrilateral elements has been reported in [45,46].

1.3. Nonlinear residual distribution schemes

The construction of high-order schemes for systems is yet another open problem. The success of the PSI scheme of Struijs [9] for the solution of steady scalar advection is still far from being achieved for nonlinear systems, and issues of robustness and generality are still to be solved. Different techniques can be found in the literature. One of these is based on the combination of a linear second-order scheme with a linear positive scheme (usually the N scheme) through a Flux-Corrected-Transport (FCT) technique or through a variant of this technique [17,24–27,47]. The main problem of this approach is that it generally shows a lack of robustness and it is theoretically very unsatisfactory due to its non-compact character. A different way of constructing nonlinear $\mathscr{RD}$ schemes is to blend locally the N scheme with a second-order linear scheme. The local nature of the blending preserves the compact character of the schemes obtained in this way, while a proper design of the blending function can guarantee both high order of accuracy and a non-oscillatory approximation of shocks. The definition of this function is however not easy. An ad hoc definition, which however has proved to be numerically very effective, is proposed in [12], while a more involved definition based on positivity and entropy stability considerations can be found in [15]. These *blended* schemes are very competitive in terms of accuracy with high-order finite volume schemes [15,42]. Nevertheless a more robust and general approach has been proposed lately by Abgrall et al. in [33,41–43,48]. The basic idea of the technique introduced in the references is to generate nonlinear schemes by locally mapping the residual of a linear positive scheme. The nonlinearity is hidden into the definition of the mapping which has the property of preserving the sign of its arguments, thus preserving positivity. The application of this technique to steady and time-dependent conservation laws has shown improved robustness and accuracy with respect to the blending approach [41–43,33].

1.4. Scopes and structure of the paper

This paper is an attempt to deal with all the issues discussed in the previous subsections by combining, analyzing and further developing some of the ideas present in the literature. We propose high-order

schemes for the approximation of time-dependent conservation laws which are conservative and do not require a multidimensional Roe linearization. We further develop the space–time $\mathscr{RD}$ schemes of [31–33,43,35] by providing a space–time $\mathscr{CRD}$ framework within which we construct conservative variants of the first-order linear monotone space–time schemes presented in the references. The linear first-order schemes obtained in this way show a very robust and non-oscillatory behavior in presence of strong discontinuities and can be used to discretize general conservation laws and as a basis to construct nonlinear high-order schemes. To this end, we analyze the technique proposed in [33,41–43,48] to construct nonlinear schemes, underlining its limits of applicability and formulating conditions for its well-posedness. As we show in the paper, these conditions are met *by construction* by the $\mathscr{CRD}$ linear schemes. Hence, the conservative formulation solves simultaneously two problems: it provides conservative non-oscillatory first-order schemes for general systems and it guarantees the well-posedness of the limiting proposed in [33,41–43,48], allowing us to construct nonlinear, conservative, high-order non-oscillatory schemes for general systems. The results presented in the paper show encouraging features of the schemes proposed: conservation, generality, robustness, oscillation free capturing of discontinuities and high resolution of complex flow structures.

The paper is organized as follows. In Section 2 we give some definitions and introduce the notation used in the sub-sequent sections. The review of $\mathscr{RD}$ and space–time $\mathscr{RD}$ schemes is done in Section 3. The conservative space–time $\mathscr{CRD}$ framework is finally introduced in Section 4. We then consider the construction of nonlinear $\mathscr{RD}$. The limiting procedure of [33,41–43,48] is analyzed in detail in Section 5, where the nonlinear schemes used in the computations are also introduced. Section 6 is devoted to the discussion of the numerical results. We assess shock capturing capabilities, robustness and accuracy of linear and nonlinear schemes on the solution of the Euler equations for a perfect gas. Finally, we show their application to a system of conservation laws modeling homogeneous two-phase flow and lacking a conservative linearization. We conclude the paper with a summary and some remarks.

2. Problem statement, definitions and labeling

In this section we introduce the notation used throughout the paper and give some basic definitions related to the mesh geometry, to the approximation of the unknowns and to the flux Jacobians. Even if a review of the basics of residual distribution is done in Section 3, we assume the reader to be somehow familiar with the work of [31–33,35]. The objective of this section is then to unify labeling and notation in order to be able to present the work reported in the references.

2.1. Generalities

In this paper we consider the numerical approximation of unsteady solutions of systems of conservation laws of the form

$$\frac{\partial \mathbf{u}}{\partial t} + \nabla \cdot \mathscr{F}(\mathbf{u}) = 0 \quad \text{on } \Omega \times [t_0, t_f] \subset \mathbb{R}^d \times \mathbb{R}^+, \tag{1}$$

where $\mathbf{u}(x_1, \ldots, x_d, t)$ is a vector of p conserved quantities, $\mathscr{F} = (\mathbf{F}_1, \ldots, \mathbf{F}_d)$ is the tensor of the conservative fluxes and $\Omega \times [t_0, t_f] \subset \mathbb{R}^d \times \mathbb{R}^+$ the space–time domain on which we seek solutions of (1). Throughout the paper we consider the two-dimensional case $d = 2$, implying $(x_1, x_2, t) = (x, y, t)$ and $\mathscr{F} = (\mathbf{F}, \mathbf{G})$, but the extension of the results to three dimensions is trivial. System (1) is supplemented with a set of boundary conditions on $\partial\Omega$ and with an initial condition $\mathbf{u}(x, y, t_0) = \mathbf{u}_0(x, y)$. We assume that (1) is hyperbolic in time. As a consequence, rewriting the system in its quasi-linear form

$$\frac{\partial \mathbf{u}}{\partial t}+\frac{\partial \mathbf{F}}{\partial \mathbf{u}}\frac{\partial \mathbf{u}}{\partial x}+\frac{\partial \mathbf{G}}{\partial \mathbf{u}}\frac{\partial \mathbf{u}}{\partial y}=0, \tag{2}$$

the matrix

$$K(\vec{\xi},\mathbf{u})=\frac{\partial \mathbf{F}}{\partial \mathbf{u}}(\mathbf{u})\xi_x+\frac{\partial \mathbf{G}}{\partial \mathbf{u}}(\mathbf{u})\xi_y=\frac{\partial \mathscr{F}}{\partial \mathbf{u}}(\mathbf{u})\cdot\vec{\xi} \tag{3}$$

has a complete set of real eigenvalues and real linearly independent eigenvectors $\forall\vec{\xi}=(\xi_x,\xi_y)\in\mathbb{R}^2$. Diagonalization of matrix $K(\vec{\xi},\mathbf{u})$ yields

$$K(\vec{\xi},\mathbf{u})=R(\vec{\xi},\mathbf{u})\Lambda(\vec{\xi},\mathbf{u})\left(R(\vec{\xi},\mathbf{u})\right)^{-1}, \tag{4}$$

where $\Lambda(\vec{\xi},\mathbf{u})$ denotes the diagonal matrix of the eigenvalues of $K(\vec{\xi},\mathbf{u})$ and $R(\vec{\xi},\mathbf{u})$ the matrix of its right eigenvectors. The choice $p=1$, $\mathbf{u}=u$ and $\mathscr{F}(\mathbf{u})=\mathscr{F}(u)=\vec{\lambda}u$, leads to the case of linear scalar advection with constant speed $\vec{\lambda}$, considered in Section 3. In this case, we simply have

$$K(\vec{\xi},\mathbf{u})=k(\vec{\xi},u)=\vec{\lambda}\cdot\vec{\xi}. \tag{5}$$

2.2. Mesh geometry

Consider an unstructured discretization of the spatial domain Ω composed by non-overlapping triangular elements. We denote the grid by τ_h, h being a reference element length (e.g. the largest element diameter), and by T the generic triangle in τ_h. The area of T is denoted by $|T|$. Given a node j in an element T, $\vec{n}_j$ denotes the inward pointing vector normal to the edge of T opposite to j, scaled by the length of the edge (see Fig. 1). For every node i in the mesh, $\mathscr{D}_i$ denotes the subset of triangles containing i and S_i is the median dual cell obtained by joining the gravity centers of the triangles in $\mathscr{D}_i$ with the midpoints of the edges meeting in i (Fig. 1). The area of S_i is denoted by $|S_i|$ and given by

$$|S_i|=\sum_{T\in\mathscr{D}_i}\frac{|T|}{3}. \tag{6}$$

The temporal domain $[t_0,t_f]$ is instead discretized by a sequence of M discrete time levels $\{t^1=t_0,t^2,\ldots,t^n,t^{n+1},\ldots,t^M=t_f\}$. The space–time schemes will be introduced with reference to a generic space–time slab $\Omega\times[t^n,t^{n+1}]$. The *time-width* of the slab is given by the time step

$$\Delta t=t^{n+1}-t^n. \tag{7}$$

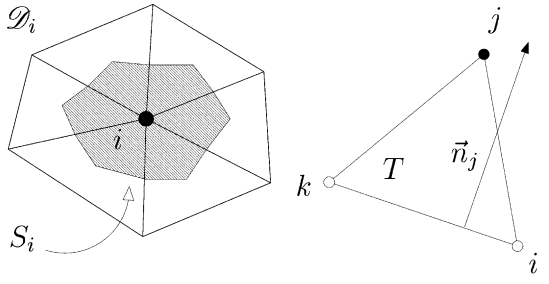

Fig. 1. Median dual cell S_i and nodal normal $\vec{n}_j$.

2.3. Variable and flux approximation

The *numerical approximation* of the unknown $\mathbf{u}$ on τ_h and in time is denoted by $\mathbf{u}^h(x, y, t)$. Denoting the continuous piecewise linear basis functions used in P^1 Finite Element methods by N_i and introducing the numerical approximations of $\mathbf{u}$ in space

$$\mathbf{u}^n(x,y) = \sum_{i\in\tau_h} N_i \mathbf{u}_i^n, \quad \mathbf{u}^{n+1}(x,y) = \sum_{i\in\tau_h} N_i \mathbf{u}_i^{n+1}, \tag{8}$$

on the space–time slab $\Omega\times[t^n, t^{n+1}]$ we assume

$$\mathbf{u}^h(x,y,t) = \frac{t-t^n}{\Delta t}\mathbf{u}^{n+1} + \frac{t^{n+1}-t}{\Delta t}\mathbf{u}^n. \tag{9}$$

The numerical approximation of the fluxes, denoted by $\mathscr{F}^h$, is given by [32–34]

$$\mathscr{F}^h = \frac{t-t^n}{\Delta t}\mathscr{F}(\mathbf{u}^{n+1}) + \frac{t^{n+1}-t}{\Delta t}\mathscr{F}(\mathbf{u}^n). \tag{10}$$

2.4. Flux jacobians

The jacobians used in the definition of the schemes are introduced here. With the notation of (3), we define on the generic element T the matrix

$$K_j = \frac{1}{2}K(\vec{n}_j, \bar{\mathbf{u}}), \tag{11}$$

where $\bar{\mathbf{u}}$ is an average value of $\mathbf{u}$ over T. Not that, for simplicity of notation, we omit to use a superscript T referring to the element in which K_j is defined, this being always clear from the context. We also introduce the following *multidimensional upwind parameters*:

$$K_j^{\pm} = R_j \Lambda_j^{\pm} (R_j)^{-1}, \tag{12}$$

where $R_j = R(\vec{n}_j, \bar{\mathbf{u}})$, $\Lambda_j = \Lambda(\vec{n}_j, \bar{\mathbf{u}})/2$ and $\Lambda_j^{\pm}$ is the diagonal matrix containing only the positive (resp. negative) entries of Λ_j. Because of the hypotheses made on the hyperbolicity of (1), the existence of $K_j^{\pm}$ is always guaranteed. In the scalar case the upwind parameters become

$$k_j^+ = \max(0, k_j), \quad k_j^- = \min(0, k_j); \qquad k_j = \frac{\lambda\cdot\vec{n}_j}{2}. \tag{13}$$

We also need to define the space–time analogs of the upwind parameters (12) needed for the space–time schemes of [35]. Denoting the $p\times p$ identity matrix by $\mathbf{I}$, we first introduce the following matrices:

$$\widetilde{K}_j = \frac{\Delta t}{2}K_j + \frac{|T|}{3}\mathbf{I}, \quad \widehat{K}_j = \frac{\Delta t}{2}K_j - \frac{|T|}{3}\mathbf{I}. \tag{14}$$

The relation between the $\widetilde{K}_j$ and $\widehat{K}_j$ matrices and the jacobians of the space–time flux $(\mathscr{F}, \mathbf{u})$ can be found in [35]. It can be easily verified that these matrices share with the K_j matrices (11) the same right and left eigenvectors and one can write

$$\widetilde{K}_j = R_j \widetilde{\Lambda}_j (R_j)^{-1}, \quad \widehat{K}_j = R_j \widehat{\Lambda}_j (R_j)^{-1} \tag{15}$$

with

$$\widetilde{\Lambda}_j = \frac{\Delta t}{2}\Lambda_j + \frac{|T|}{3}\mathbf{I}, \quad \widehat{\Lambda}_j = \frac{\Delta t}{2}\Lambda_j - \frac{|T|}{3}\mathbf{I}. \tag{16}$$

We define then the *space–time multidimensional upwind parameters* [35]

$$\widetilde{K}_j^{\pm} = R_j \widetilde{\Lambda}_j^{\pm} (R_j)^{-1}, \quad \widehat{K}_j^{\pm} = R_j \widehat{\Lambda}_j^{\pm} (R_j)^{-1}, \tag{17}$$

where $\widetilde{\Lambda}_j^{\pm}$ and $\widehat{\Lambda}_j^{\pm}$ are diagonal matrices containing only the positive (resp. negative) entries of $\widetilde{\Lambda}_j$ and $\widehat{\Lambda}_j$ respectively. In the case of scalar advection the previous definitions become

$$\widetilde{k}_j^{+} = \max(0, \widetilde{k}_j), \quad \widetilde{k}_j^{-} = \min(0, \widetilde{k}_j) \qquad \text{with } \widetilde{k}_j = \frac{\Delta t}{2} k_j + \frac{|T|}{3} \tag{18}$$

and

$$\widehat{k}_j^{+} = \max(0, \widehat{k}_j), \quad \widehat{k}_j^{-} = \min(0, \widehat{k}_j) \qquad \text{with } \widehat{k}_j = \frac{\Delta t}{2} k_j - \frac{|T|}{3}. \tag{19}$$

3. Residual distribution schemes

This section is devoted to the description of the basics of $\mathscr{RD}$. We start with the simplified case of linear constant advection

$$\frac{\partial u}{\partial t} + \vec{\lambda} \cdot \nabla u = 0 \quad \text{on } \Omega \times [t_0, t_f] \subset \mathbb{R}^2 \times \mathbb{R}^+. \tag{20}$$

We first consider the case of steady advection ($t_f \to \infty$) and then we recall the space–time schemes on prisms [31–33,35]. The extension to systems and nonlinear conservation laws is then discussed. The content of these pages being far from exhaustive, the reader can refer to the extensive bibliography given in the introduction for a more complete overview on $\mathscr{RD}$.

3.1. Steady scalar advection

Consider the numerical solution of the steady limit of (20). The $\mathscr{RD}$ discretization procedure consists of the three following steps [2]:

(1) In every element $T \in \tau_h$ we compute the *residual* or *fluctuation*

$$\phi^h = \int_T \vec{\lambda} \cdot \nabla u^h \, \mathrm{d}x \, \mathrm{d}y. \tag{21}$$

Taking $u^h = u^n$ (see Eq. (8)), the residual can be shown to be

$$\phi^h = \sum_{j \in T} k_j u_j^n. \tag{22}$$

(2) ϕ^h is distributed to (split among) the nodes of the element. The fraction of ϕ^h sent to node $i \in T$ is denoted by ϕ_i^T and is referred to as the *local nodal residual* or *distribution function*. It is also customary to define the *distribution coefficients* $\{\beta_j\}_{j \in T}$:

$$\beta_i = \frac{\phi_i^T}{\phi^h}. \tag{23}$$

(3) The solution is updated according to the explicit iterative scheme

$$u_i^{n+1} = u_i^n - \frac{\Delta t}{|S_i|} \sum_{T \in \mathscr{D}_i} \phi_i^T = u_i^n - \frac{\Delta t}{|S_i|} \sum_{T \in \mathscr{D}_i} \beta_i \phi^h. \tag{24}$$

The properties of the discretization are determined by the choice of the distribution functions. The following properties are relevant to our scopes:

Consistency. The local nodal residuals *must* respect the constraint

$$\sum_{j\in T}\phi_j^T = \phi^h. \tag{25}$$

The consistency requirement can be equivalently expressed as

$$\sum_{j\in T}\beta_j = 1. \tag{26}$$

Linearity. A scheme is *linear* if

$$\phi_i^T = \sum_{j\in T} c_{ij}u_j^n \tag{27}$$

with all the c_{ij} coefficients independent on the numerical solution.

Multidimensional upwinding. If node i is located upstream in a triangle with respect to $\vec{\lambda}$, then $k_i < 0$. A scheme is *multidimensional upwind* if

$$k_i \leqslant 0 \;\Rightarrow\; \phi_i^T = 0. \tag{28}$$

Linearity preservation. *Linearity preserving* schemes preserve piecewise linear exact steady solutions of (20), hence they are second-order accurate. In [15,42,48] is shown that in 2D, if the mesh is regular enough, a sufficient condition for a $\mathscr{RD}$ scheme to be second-order accurate is that

$$\phi_i^T = \mathscr{O}(h^3), \tag{29}$$

which is obtained if the approximation of the fluxes $\mathscr{F}^h = \vec{\lambda}u^h$ in (21) is at least second-order accurate and if the distribution coefficients are bounded. As a consequence, if

$$\lim_{\phi^h\to 0}\beta_i\phi^h = \lim_{\phi^h\to 0}\phi_i^T = 0 \Longleftrightarrow |\beta_i| < \infty, \tag{30}$$

then the scheme is linearity preserving, hence second-order accurate.

Positivity. Making use of (27), we can rewrite the update (24) as

$$u_i^{n+1} = u_i^n - \frac{\Delta t}{|S_i|}\sum_{T\in\mathscr{D}_i}\sum_{j\in T} c_{ij}u_j^n. \tag{31}$$

A scheme is *positive* if

$$\sum_{T\in\mathscr{D}_i\cap\mathscr{D}_j} c_{ij} \leqslant 0, \quad \sum_{T\in\mathscr{D}_i} c_{ii} \geqslant 0, \quad \Delta t\sum_{T\in\mathscr{D}_i} c_{ii} \leqslant |S_i|. \tag{32}$$

Positive schemes respect a *local discrete maximum principle* [49] and are of fundamental importance for the approximation of discontinuous solutions. We denote by CFL the ratio

$$\mathrm{CFL} = \frac{\Delta t\sum_{T\in\mathscr{D}_i} c_{ii}}{|S_i|}. \tag{33}$$

An analog of Godunov's theorem for Residual Distribution [10,43,42,50] states that *a linear scheme cannot be simultaneously positive and linearity preserving*. Nonlinear schemes are then needed to combine these two properties.

3.1.1. The linear positive N scheme

It is useful to introduce the linear positive scheme at the basis of our work. The so-called N scheme is defined by the distribution function

$$\phi_i^{\mathrm{N}} = k_i^+(u_i - u_{\mathrm{in}}), \tag{34}$$

where the *inflow state* u_{in} is the linearly interpolated value of u^h in the upstream point of intersection between the streamline crossing element T and the element itself (see Fig. 2) and is given by [2]

$$u_{\mathrm{in}} = -N^{-1}\sum_{j\in T} k_j^- u_j, \quad N = \sum_{j\in T} k_j^+. \tag{35}$$

Note that introducing the *outflow state* u_{out} (see Fig. 2)

$$u_{\mathrm{out}} = N^{-1}\sum_{j\in T} k_j^+ u_j, \tag{36}$$

and using expression (22), one can easily show that [2]

$$\phi^h = \sum_{j\in T} k_j u_j = N(u_{\mathrm{out}} - u_{in}) = \sum_{j\in T}\phi_j^{\mathrm{N}}. \tag{37}$$

Hence the N scheme is consistent if the residual can be expressed as in (22), that is provided that we can use the flux jacobians k_j to compute ϕ^h. The N scheme, initially introduced by Roe [36,37], is multidimensional upwind and positive under the constraint (see Eq. (32))

$$\Delta t \sum_{T\in\mathscr{D}_i} k_i^+ \leqslant |S_i|. \tag{38}$$

Being positive and linear, the scheme is not linearity preserving. Note also that the quantity N in (35) approaches zero as $\vec{\lambda} \to 0$. Even though in this case $\phi^h \to 0$ and $\phi_j^{\mathrm{N}} \to 0\ \forall j \in T$, and even if $k_j N^{-1}$ and $k_j^{\pm} N^{-1}$ remain well behaved [15], care must be taken to avoid division by zero in this limit.

3.2. Time-dependent scalar advection

Consider now the solution of (20) in the time-dependent case. Given the nodal values of the numerical solution at time t^n, $\{u_i^n\}_{i\in\tau_h}$, the space–time $\mathscr{RD}$ solution procedure to compute $\{u_i^{n+1}\}_{i\in\tau_h}$ can be summarized in three steps:

(1) $\forall T \in \tau_h$ the following *space–time residual* is computed:

$$\phi^h = \int_{t^n}^{t^{n+1}} \int_T \left(\frac{\partial u^h}{\partial t} + \vec{\lambda}\cdot\nabla u^h\right) \mathrm{d}x\,\mathrm{d}y\,\mathrm{d}t. \tag{39}$$

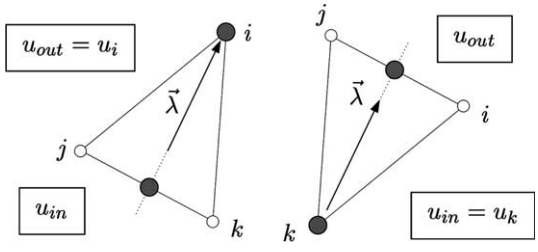

Fig. 2. Inflow and outflow states.

Using (9) and the properties of the P^1 basis functions N_i, the space–time residual can be shown to be [33]

$$\phi^h = \sum_{j\in T} \frac{|T|}{3}\left(u_j^{n+1} - u_j^n\right) + \frac{\Delta t}{2}\sum_{j\in T} k_j u_j^n + \frac{\Delta t}{2}\sum_{j\in T} k_j u_j^{n+1}. \tag{40}$$

Definition (39) of the residual renders the schemes inherently implicit. Introducing the modified parameters (18) and (19), the space–time residual can be expressed in the more compact form [35,51]

$$\phi^h = \sum_{j\in T}\left(\widehat{k}_j u_j^n + \widetilde{k}_j u_j^{n+1}\right). \tag{41}$$

As shown in [35,51], the parameters (18) and (19) are space–time analogs of the k_j parameters (13).

(2) Portions of the cell residual are distributed to the nodes of T. The fraction of ϕ^h distributed to a node $i \in T$ is denoted by ϕ_i^T. Again, one introduces distribution coefficients given by (23).

(3) The unknowns $\{u_i^{n+1}\}_{i\in\tau_h}$ are the solution of the algebraic system

$$\sum_{T\in\mathscr{D}_i} \phi_i^T = 0 \quad \forall i \in \tau_h. \tag{42}$$

We must specify the form of the distribution functions $\{\phi_j^T\}_{j\in T}$ to determine the properties of the discretization. The definitions of consistency, linearity and linearity preservation remain basically unchanged. Schemes having bounded distribution coefficients can be shown to be second-order accurate in space and time, provided that the approximations of the unknown and of the fluxes, u^h and $\mathscr{F}^h$ respectively, are at least second-order accurate in space and time [33,43]. The following two properties need instead a specific definition:

Causality. It corresponds to the preservation of the *past* solution. For all the schemes respecting this property only the nodal values at time t^{n+1} receive portions of the residual, hence only the values $\{u_i^{n+1}\}_{i\in\tau_h}$ are considered as unknowns in (42). This property can be shown to be strictly tied to multidimensional upwinding in space–time [29,30,35,51]. All the schemes considered in this paper respect causality.

Positivity. Introducing the arrays $\mathbf{U}^n$ and $\mathbf{U}^{n+1}$, with $\mathbf{U}_i^k = u_i^k \ \forall i \in \tau_h$ and $k = n, n+1$, system (42) can be rewritten as

$$\mathscr{A}\mathbf{U}^{n+1} = \mathscr{B}\mathbf{U}^n. \tag{43}$$

Positive space–time $\mathscr{RD}$ respect simultaneously the following properties:

(1) $\mathscr{A}$ is an invertible $\mathscr{M}$-matrix ($\mathscr{A}_{ii} \geqslant 0, \mathscr{A}_{ij} \leqslant 0, |\mathscr{A}_{ii}| > \sum_j |\mathscr{A}_{ij}| \ \forall i$).
(2) $\mathscr{B}$ is a positive matrix ($\mathscr{B}_{ij} \geqslant 0 \ \forall i, j$).

Positive space–time schemes respect a discrete maximum principle [33].

Due to Godunov's theorem only nonlinear space–time schemes can be simultaneously positive and linearity preserving.

3.2.1. Linear positive space–time schemes: the N1 and N2 schemes

We present here the space–time positive schemes used in our work. They have been proposed in [35,31–33] and they are different extensions of the N scheme (34) to the space–time framework.

3.2.2. The N1 scheme of Csík et al.

As remarked in the introduction, the extension of the space–time framework introduced in [28–30] to prismatic elements has been reported in [35]. The N1 scheme, is the space–time variant of the N scheme

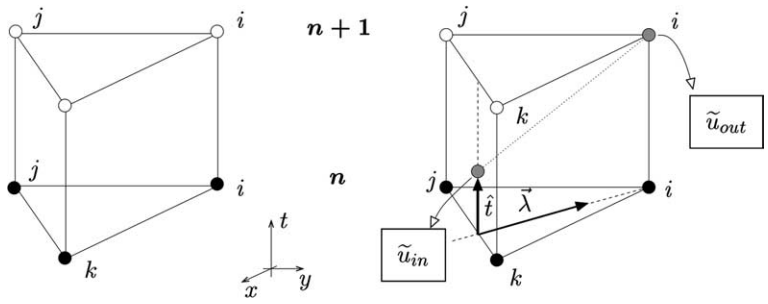

Fig. 3. Space–time element (left). Space–time inflow and outflow states (right).

proposed in the reference. Consider a triangle T composed of nodes (i, j, k) and the corresponding space–time element $T\times[t^n, t^{n+1}]$ (left in Fig. 3). We define space–time inflow and outflow states as the values of u^h at the intersections of the characteristic line crossing the space–time element and the element itself (right in Fig. 3):

$$\widetilde{u}_{\text{in}} = -\widetilde{N}^{-1}\sum_{j\in T}\left(\widetilde{k}_j^- u_n^{n+1} + \widehat{k}_j^- u_j^n\right), \quad \widetilde{u}_{\text{out}} = \widetilde{N}^{-1}\sum_{j\in T}\left(\widetilde{k}_j^+ u_n^{n+1} + \widehat{k}_j^+ u_j^n\right) \tag{44}$$

with $\widetilde{N}$ given by

$$\widetilde{N} = \sum_{j\in T}\left(\widetilde{k}_j^+ + \widehat{k}_j^+\right). \tag{45}$$

With these definitions, one can easily show that (41) can be rewritten as

$$\phi^h = \sum_{j\in T}\left(\widehat{k}_j u_j^n + \widetilde{k}_j u_j^{n+1}\right) = \widetilde{N}(\widetilde{u}_{\text{out}} - \widetilde{u}_{\text{in}}). \tag{46}$$

The N1 scheme is then defined by the distribution functions

$$\begin{aligned} \phi_i^{\text{N1}} &= \widetilde{k}_i^+(u_i^{n+1} - \widetilde{u}_{\text{in}}) \quad \text{to node } i \text{ at time } t^{n+1}, \\ \phi_i^{\text{N1}} &= \widehat{k}_i^+\left(u_i^n - \widetilde{u}_{\text{in}}\right) \quad \text{to node } i \text{ at time } t^n. \end{aligned} \tag{47}$$

The N1 scheme is a true space–time variant of the N scheme in which the $\widetilde{k}_j$ and $\widehat{k}_j$ parameters play the role of Jacobians of the space–time flux $\vec{\lambda}u + \hat{t}u$ (see Fig. 3). Indeed, $\widetilde{k}_j$ contains a contribution proportional to k_j, which is the Jacobian of the spatial components of the flux, and an extra term proportional to the Jacobian of the temporal flux:

$$\widetilde{k}_j = \underbrace{\frac{\Delta t}{2}k_j}_{\text{spatial component}} + \underbrace{\frac{|T|}{3}}_{\text{temporal component}}. \tag{48}$$

A similar decomposition can be done for $\widehat{k}_j$. Since the Jacobian of the temporal component of the fluxes never vanishes, the N1 scheme is always well defined, $\widetilde{N}$ in (45) remaining positive when $\vec{\lambda}\to 0$. So, differently from the N scheme, the N1 scheme does not need any fix in this limit. Moreover, it is positive and it inherits all the stability properties of its steady counterpart. Evidently, as written in (51), the N1 scheme does not respect causality unless one has

$$\widehat{k}_j^+ = 0 \quad \forall j \in T, \forall T \in \tau_h. \tag{49}$$

This condition highlights the relation between causality and multidimensional upwinding in space–time. It can be immediately checked that (49) implies

$$\Delta t \leqslant \min_{T\in\tau_h} \Delta t_T, \quad \Delta t_T = \frac{2}{3}\frac{|T|}{\max\limits_{j\in T} k_j^+}. \tag{50}$$

Hence the N1 scheme respects causality under a time-step constraint. Note that if (49) is respected, then no residual is distributed to nodes at time level t^n and the N1 scheme becomes

$$\phi_i^{\mathrm{N1}} = \widetilde{k}_i^+ (u_i^{n+1} - \widetilde{u}_{\mathrm{in}}) \tag{51}$$

with

$$\widetilde{u}_{\mathrm{in}} = -\widetilde{N}^{-1} \sum_{j\in T} \left(\widetilde{k}_j^- u_n^{n+1} + \widehat{k}_j^- u_j^n \right), \quad \widetilde{N} = \sum_{j\in T} \widetilde{k}_j^+. \tag{52}$$

Condition (50) is a strict constraint for an implicit scheme. However, in [28–30,35] it has been overcome using a double layer formulation in which one solves simultaneously for values of u^h at time $t^{n+\alpha}$ and t^{n+1}, with $\alpha \in (0, 1)$. Causality is guaranteed by the satisfaction of (50) in the first layer of elements, while an arbitrarily large time step $t^{n+1} - t^{n+\alpha}$ can be used in the second layer. This technique increases the number of unknowns to be solved for at each time step but it allows to construct unconditionally stable and positive schemes [29,30,35]. This is of great advantage when dealing with *locally* highly refined meshes as proved in [28,29,35]. As already remarked, due to its true space–time character, the N1 scheme is always well defined. However, the additional numerical dissipation due to the upwinding in the time direction results in a very strong numerical dissipation as shown by the results reported in [35].

3.2.3. The N2 scheme of Abgrall and Mezine

A different linear positive scheme has been introduced in [32,33]. With the notation of (34), the N2 scheme is defined by the following local nodal residuals:

$$\phi_i^{\mathrm{N2}} = \frac{|T|}{3}\left(u_i^{n+1} - u_i^n\right) + \frac{\Delta t}{2} k_i^+ \left(u_i^n - u_{\mathrm{in}}^n\right) + \frac{\Delta t}{2} k_i^+ \left(u_i^{n+1} - u_{\mathrm{in}}^{n+1}\right). \tag{53}$$

Even if proposed in the space–time framework, the N2 scheme is the combination of the Crank–Nicholson time-integration with the N scheme (34). It is consistent and it verifies causality by construction. The N2 scheme is positive under the time step constraint:

$$\Delta t \sum_{T\in\mathscr{D}_i} k_i^+ \leqslant 2|S_i|. \tag{54}$$

Not surprisingly, condition (54) is the time-step restriction for the positivity of the N scheme (38) with CFL = 2, typical of the Crank–Nicholson time discretization [52]. Using the double layer approach of [29,30,35] the time-step constraint has been overcome in [33,43,34] where unconditionally stable and positive variants of the scheme have been presented. The application of these variants to computations on meshes containing highly refined areas has been shown in the references. As for the N scheme, in the limit $\vec{\lambda} \to 0$, a fix is needed to avoid division by zero.

3.3. Matrix residual distribution for linear hyperbolic systems

The extension of $\mathscr{RD}$ to the numerical solution of hyperbolic systems can be designed following different approaches. Here we adopt the so-called *matrix* variant of the schemes [5,12,13]. Matrix $\mathscr{RD}$ are a formal extension of the scalar schemes to systems. In particular, if $\mathscr{F}$ in (1) is linear in $\mathbf{u}$, then the K_j matrices (11)

are constant and the schemes presented in Sections 3 and 5 can be applied as they are, provided that the k_j parameters are replaced by the K_j matrices and the scalar unknown u^h is replaced by a vector unknown $\mathbf{u}^h$. To give an example, the matrix variant of the N scheme (34) is defined by the distribution function

$$\phi_i^{\mathrm{N}} = K_i^+(\mathbf{u}_i - \mathbf{u}_{\mathrm{in}}), \quad \mathbf{u}_{\mathrm{in}} = -N^{-1}\sum_{j\in T} K_j^-\mathbf{u}_j, \tag{55}$$

where now N is the matrix

$$N = \sum_{j\in T} K_j^+, \tag{56}$$

and the element residual is given by

$$\phi^h = \sum_{j\in T} K_j\mathbf{u}_j. \tag{57}$$

The distribution coefficients become distribution matrices. Properties such as consistency, linearity and linearity preservation extend quite easily to the matrix schemes. The same is not true for positivity for which no *matrix* analog can be formulated. However, a discussion concerning the stability properties of matrix $\mathscr{RD}$ schemes can be found in [41–43], where the authors use a wave decomposition technique to derive L_∞–bounds on the numerical solution obtained with the matrix variant of some positive scalar schemes.

Matrix space–time residual distribution schemes are obtained in a similar fashion. As for the matrix $\mathscr{RD}$, properties such as consistency, linearity, linearity preservation and causality extend trivially to the system case. No definition of a positive scheme can be given, even though the wave decomposition analysis of [41–43] could be applied. As an example, the matrix variant of the space–time N1 scheme (51) is defined by the local nodal residuals

$$\begin{aligned} \phi_i^{\mathrm{N1}} &= \widetilde{K}_i^+(\mathbf{u}_i^{n+1} - \widetilde{\mathbf{u}}_{\mathrm{in}}) \quad \text{to node } i \text{ at time level } t^{n+1},\\ \phi_i^{\mathrm{N1}} &= \widehat{K}_i^+\left(\mathbf{u}_i^{n} - \widetilde{\mathbf{u}}_{\mathrm{in}}\right) \quad \text{to node } i \text{ at time level } t^{n} \end{aligned} \tag{58}$$

with

$$\widetilde{\mathbf{u}}_{\mathrm{in}} = -\widetilde{N}^{-1}\sum_{j\in T}\left(\widetilde{K}_j^+\mathbf{u}_j^{n+1} + \widehat{K}_j^+\mathbf{u}_j^n\right), \quad \widetilde{N} = \sum_{j\in T}\left(\widetilde{K}_j^+ + \widehat{K}_j^+\right) \tag{59}$$

and the space–time residual given by

$$\phi^h = \sum_{j\in T}\left(\widetilde{K}_j\mathbf{u}_j^{n+1} + \widehat{K}_j\mathbf{u}_j^n\right). \tag{60}$$

The causality constraint (50) becomes for the matrix N1 scheme

$$\Delta t \leqslant \min_{t\in\tau_h}\Delta t_T, \quad \Delta t_T = \frac{2}{3}\frac{|T|}{\max_{j\in T}\max_k \lambda_{jk}^+}, \tag{61}$$

being λ_{jk} the kth eigenvalue of K_j. Note that if constraint (61) is respected, all the $\widehat{K}_j^+$ are zero and the N1 scheme simply becomes

$$\phi_i^{\mathrm{N1}} = \widetilde{K}_i^+\left(\mathbf{u}_i^{n+1} - \widetilde{\mathbf{u}}_{\mathrm{in}}\right) \tag{62}$$

with

$$\widetilde{\mathbf{u}}_{\mathrm{in}} = -\widetilde{N}^{-1}\sum_{j\in T}\left(\widetilde{K}_j^+\mathbf{u}_j^{n+1} + \widehat{K}_j^+\mathbf{u}_j^n\right), \quad \widetilde{N} = \sum_{j\in T}\widetilde{K}_j^+. \tag{63}$$

3.4. Conservative matrix $\mathscr{RD}$ for nonlinear systems: $\mathscr{LRD}$ vs $\mathscr{CRD}$

The extension of the schemes to the discretization of nonlinear systems is more difficult, due to the fact that nonlinear conservation laws can evolve discontinuous solutions even for smooth initial data. In this case, care must be taken to ensure that across these discontinuities the physically relevant jump conditions are recovered at the discrete level. For the Euler equations with perfect gas equation of state, the existence of a multidimensional analog of Roe's parameter vector $\mathbf{Z}$ [1,53] implies an equivalence between the quasi-linear form of the equations and their integral form:

$$\oint_{\partial T} \mathscr{F}\cdot\vec{n}\,\mathrm{d}l = \int_T \nabla\cdot\mathscr{F}\,\mathrm{d}x\,\mathrm{d}y = \int_T \left(\frac{\partial \mathbf{F}}{\partial \mathbf{Z}}(\mathbf{Z})\frac{\partial \mathbf{Z}}{\partial x} + \frac{\partial \mathbf{G}}{\partial \mathbf{Z}}(\mathbf{Z})\frac{\partial \mathbf{Z}}{\partial y}\right)\mathrm{d}x\,\mathrm{d}y. \tag{64}$$

Using the fact that the flux jacobians are linear functions of the components of $\mathbf{Z}$ and assuming a piecewise linear continuous approximation of $\mathbf{Z}$ on τ_h, last expression can be evaluated *exactly* as

$$\oint_{\partial T} \mathscr{F}\cdot\vec{n}\,\mathrm{d}l = \frac{1}{2}\sum_{j\in T}\frac{\partial \mathscr{F}}{\partial \mathbf{Z}}(\bar{\mathbf{Z}})\cdot\vec{n}_j\mathbf{Z}_j = \sum_{j\in T} K_j(\bar{\mathbf{Z}})\bar{\mathbf{u}}_j, \tag{65}$$

where $\bar{\mathbf{Z}}$ is the arithmetic average of the values of $\mathbf{Z}$ in the nodes of T and

$$K_j = \frac{1}{2}\frac{\partial \mathscr{F}}{\partial \mathbf{Z}}(\bar{\mathbf{Z}})\frac{\partial \mathbf{Z}}{\partial \mathbf{u}}(\bar{\mathbf{Z}})\cdot\vec{n}_j = \frac{1}{2}\frac{\partial \mathscr{F}}{\partial \mathbf{u}}(\bar{\mathbf{Z}})\cdot\vec{n}_j, \quad \bar{\mathbf{u}}_j = \frac{\partial \mathbf{u}}{\partial \mathbf{Z}}(\bar{\mathbf{Z}})\mathbf{Z}_j. \tag{66}$$

If Roe's linearization is used to evaluate the flux jacobians, the residual can then be still expressed as in (22). In this case, matrix $\mathscr{RD}$ schemes are obtained as in the linear case. As in [44], we refer to this class of Residual Distribution schemes as to $\mathscr{LRD}$, denoting that conservation is guaranteed by the linearization. Also in the nonlinear case, properties such as linearity preservation and consistency extend easily to the $\mathscr{LRD}$ schemes, while the linearity of a scheme is formulated in terms of the linearized problem. More complex is the issue of defining a monotonicity condition in a rigorous way, this condition being quite intuitive but very difficult to formalize, especially on general unstructured meshes. The L_∞ stability framework proposed in [41–43] for linear systems could be indeed applied to the linearized problem to define the local stability of a scheme. The equivalence with the nonlinear problem implied by the exact mean-value linearization would allow to extend the analysis to the nonlinear case. It is however out of the scopes of this paper to formally define the monotonicity of a scheme and the reader is referred to the above mentioned articles and to the lecture [49] for a discussion on the topic. Here, by abuse of language, in the nonlinear case we will refer to a matrix scheme as being monotone if it produces numerical solutions which are piecewise smooth and that, in correspondence of discontinuities and of large local variations of the solution, does not produce any unphysical oscillations. An example of such a scheme for the Euler equations is the $\mathscr{LRD}$ N scheme obtained by combining (55) with the conservative linearization of [1]. Its ability to approximate strong discontinuities without spurious numerical oscillations has made this scheme the basis for the construction of most (or all) the nonlinear high-order schemes proposed in the literature. Similarly, in [32,33,43] an $\mathscr{LRD}$ N2 scheme for the Euler equations has been proposed. Under a constraint analog to (61) the scheme of [32,33,43] yields oscillation free shock capturing of moving discontinuities.

When a conservative linearization cannot be used, the $\mathscr{LRD}$ matrix N scheme and its space–time variants cannot be conservative. As mentioned in the introduction, the need of monotone matrix schemes for the solution of general systems, has led to several generalizations of the N scheme the most appealing of which are the N scheme based on adaptive numerical quadrature of the quasi-linear form of [40] and the $\mathscr{CRD}$ approach of [44]. The technique proposed in the second reference, and used here, is briefly recalled hereafter.

The approach proposed in [44] is inspired by the observation that the inflow state $\mathbf{u}_{\text{in}}$ in (55) is uniquely defined by the conditions

$$\begin{cases} \phi_i = K_i^+(\mathbf{u}_i - \mathbf{u}_{\text{in}}), \\ \sum_{j\in T} \phi_j = \phi^h = \sum_{j\in T} K_j \mathbf{u}_j. \end{cases} \tag{67}$$

As a consequence, conservative first-order schemes can be defined by

$$\begin{cases} \phi_i = K_i^+(\bar{\mathbf{u}})(\mathbf{u}_i - \mathbf{u}_c), \\ \sum_{j\in T} \phi_j = \phi^h = \oint_{\partial T} \mathscr{F}^h \cdot \vec{n}\, \mathrm{d}l, \end{cases} \tag{68}$$

where the last integral can be approximated using quadrature formulas on the edges of T. The parameter selecting a particular scheme is the linearized state $\bar{\mathbf{u}}$ used to evaluate the flux jacobians. However, the schemes are conservative independently on the choice of $\bar{\mathbf{u}}$, due to the evaluation of the residual ϕ^h via the integration of the fluxes on the boundary of T, and to the definition of $\mathbf{u}_c$: once $\bar{\mathbf{u}}$ is chosen, in fact, $\mathbf{u}_c$ is uniquely defined and given by

$$\mathbf{u}_c = N^{-1}\left(\sum_{j\in T} K_j^+ \mathbf{u}_j - \phi^h\right). \tag{69}$$

The authors of [44] have introduced the terminology $\mathscr{CRD}$ to denote the class of $\mathscr{RD}$ schemes for which conservation is guaranteed by computing the residual with the direct evaluation of the contour integral of the fluxes, as opposed to the $\mathscr{LRD}$ approach described earlier. Compared to the N scheme based on adaptive quadrature of [40], the $\mathscr{CRD}$ N scheme is considerably cheaper and still yields non-oscillatory solutions.[1] Nevertheless, no theoretical analysis has been done for the $\mathscr{CRD}$ N scheme. As already mentioned, in [40] the authors prove energy and entropy stability of their scheme, while L_∞ stability can be proved using the wave decomposition technique of [41–43].

4. Conservative schemes for time-dependent systems

In this section we propose a conservative framework allowing to approximate discontinuous solutions of general time-dependent conservation laws. In particular, we consider the construction of conservative schemes guaranteeing a non-oscillatory approximation of weak unsteady solutions of (1). As remarked in the previous section, the particular case of the Euler equations with perfect gas equation of state has been already considered in [32,33,43], where, thanks to the existence of the multidimensional conservative linearization [1], an $\mathscr{LRD}$ N2 scheme has been proposed and extensively tested. Here we consider the more general case in which such a linearization does not exist. We define on each element $T \in \mathscr{T}_h$ the space–time residual as [33]

$$\phi^h = \int_{t^n}^{t^{n+1}} \int_T \left(\frac{\partial \mathbf{u}^h}{\partial t} + \nabla \cdot \mathscr{F}^h\right) \mathrm{d}x\, \mathrm{d}y\, \mathrm{d}t. \tag{70}$$

Taking $\mathbf{u}^h$ and $\mathscr{F}^h$ as in (9) and (10), respectively, we compute (70) as

$$\phi^h = \sum_{j\in T} \frac{|T|}{3}\left(\mathbf{u}_j^{n+1} - \mathbf{u}_j^n\right) + \frac{\Delta t}{2}\oint_{\partial T} \mathscr{F}(\mathbf{u}^{n+1}) \cdot \vec{n}\, \mathrm{d}l + \frac{\Delta t}{2}\oint_{\partial T} \mathscr{F}(\mathbf{u}^n) \cdot \vec{n}\, \mathrm{d}l, \tag{71}$$

[1] In [44], a monotone Mach 10 bow shock computation on a circular cylinder is shown. The residual is computed using Simpson's rule on each edge of T, requiring in total 6 quadrature points. Only 1 Gauss point is used to compute each K_j.

where the last two integrals are approximated using Gaussian formulas. Provided that consistency is respected (see Eq. (25)), this approach guarantees the recovery of a discrete analog of the Rankine–Hugoniot conditions across unsteady shocks. In particular, conservative schemes are readily obtained defining ϕ_i as

$$\phi_i = \beta_i \phi^h, \tag{72}$$

where the $\{\beta_j\}_{j\in T}$ are distribution matrices respecting

$$\sum_{j\in T} \beta_j = \mathbf{I}. \tag{73}$$

A scheme of the form (72) is conservative independently on how the β_j matrices are defined, as long as (73) is respected. Examples of schemes of this type are the space–time LDA scheme of [35] and the LDA scheme of Caraeni [22]. These schemes are conservative linear and linearity preserving. Unfortunately, they give a very oscillatory resolution of discontinuities. The problem is then to design matrix schemes providing a non-oscillatory approximation of these features, consistent with the residual given by (71). In order to do this, the first step is the definition of linear first-order non-oscillatory schemes to be used as a basis for the construction of nonlinear schemes. This will be accomplished by constructing $\mathscr{CRD}$ variants of the N1 and N2 schemes.

The $\mathscr{CRD}$ N1 scheme. Consider first the case of the N1 scheme. As done for the N scheme in [44], we observe that a family of conservative and consistent schemes is defined by

$$\begin{cases} \phi_i^{\mathrm{N1}} = \widetilde{K}_i^+(\bar{\mathbf{u}})\left(\mathbf{u}_i^{n+1} - \widetilde{\mathbf{u}}_c\right), \\ \sum_{j\in T} \phi_j^{\mathrm{N1}} = \phi^h \end{cases} \tag{74}$$

with ϕ^h given by (71). Once the linearized state $\bar{\mathbf{u}}$ is chosen, and assuming that the causality constraint (61) is verified, $\widetilde{\mathbf{u}}_c$ is uniquely defined and given by

$$\widetilde{\mathbf{u}}_c = \widetilde{N}^{-1}\left(\sum_{j\in T} \widetilde{K}_j^+ \mathbf{u}_j^{n+1} - \phi^h\right), \quad \widetilde{N} = \sum_{j\in T} \widetilde{K}_j^+. \tag{75}$$

The $\mathscr{CRD}$ N2 scheme. The $\mathscr{CRD}$ variant of the matrix N2 scheme is readily obtained recalling that the N2 scheme is the combination of the N scheme with Crank–Nicholson time-integration. The $\mathscr{CRD}$ N2 scheme is then defined by

$$\phi_i^{\mathrm{N2}} = \frac{|T|}{3}\left(\mathbf{u}_i^{n+1} - \mathbf{u}_i^n\right) + \frac{\Delta t}{2} K_i^+\left(\mathbf{u}_i^{n+1} - \mathbf{u}_c^{n+1}\right) + \frac{\Delta t}{2} K_i^+\left(\mathbf{u}_i^n - \mathbf{u}_c^n\right) \tag{76}$$

with

$$\mathbf{u}_c^n = N^{-1}\left(\sum_{j\in T} K_j^+ \mathbf{u}_j^n - \phi^n\right), \quad \phi^n = \oint_{\partial T} \mathscr{F}(\mathbf{u}^n)\cdot \vec{n}\, \mathrm{d}l, \tag{77}$$

and similarly for $\mathbf{u}_c^{n+1}$. Note that in all the formulas $K_j = K_j(\bar{\mathbf{u}})$. Moreover, for the N2 scheme, different linearized states could be used to compute $\mathbf{u}_c^n$ and $\mathbf{u}_c^{n+1}$, even if this choice does not influence the consistency of the scheme.

The space–time schemes (74) and (76) are the conservative $\mathscr{CRD}$ variants of the matrix N1 and N2 schemes we sought. Even though we give no formal proof that these scheme verify any local stability condition, we will give extensive numerical evidence that they produce non-oscillatory approximations of discontinuous solutions and hence, that they are monotone according to the *heuristic* definition of monotonicity given in Section 3.4. In the rest of the paper, we will refer to schemes (74) and (76) simply

as to the linear N1 and linear N2 scheme. As a final remark, we note that for the systems of equations we consider in the paper, the matrix N in (77) is singular in the case of vanishing flow speed. Even though in [15] it is shown that $K_j N^{-1}$ and $K_j^+ N^{-1}$ are well behaved in this limit, in the system case this singularity does not correspond necessarily to the case $\phi^h = 0$. In these instances, the N2 scheme needs a fix to allow the inversion of N. As in the scalar case, due to its true space–time character, the N1 scheme is always well defined, since the matrix $\widetilde{N}$ has no singular points. On the other hand this also makes the scheme particularly diffusive, as it will be clear from the numerical results.

The next step is to show how to construct, starting from the linear N1 and N2 schemes, linearity preserving schemes, guaranteeing an oscillation free capturing of shocks.

5. Conservative high-order nonlinear $\mathscr{RD}$ schemes

In this section we perform an analysis of the nonlinear limiting technique proposed in [33,41–43,48] for the construction of nonlinear $\mathscr{RD}$ schemes. Nonlinear schemes are needed to combine linearity preservation and positivity or, more generally speaking, non-oscillatory shock capturing. The advantage of the use of the $\mathscr{RD}$ approach is that high-order schemes yielding a monotone (in the sense of the previous sentence) and stable approximation of shocks can be obtained on unstructured meshes without adding to the discretization local nonlinear discontinuity capturing operators. The key idea is, given a positive first-order scheme, to use the sign of its local residuals as a reference to generate a positive linearity preserving scheme. This approach has its roots in the early work of Struijs. The PSI scheme proposed in [9] still represents undoubtedly an optimum among schemes for the solution of steady scalar advection on unstructured meshes. A first generalization of the PSI scheme of [9] can be found in [54], where it is shown how nonlinear $\mathscr{RD}$ schemes can be generated through the use of limiter functions typical of high-order $\mathscr{FV}$ methods. More recently, the general mathematical framework of the *limited* or *modified* $\mathscr{RD}$ schemes has been introduced by Abgrall et al. in [33,41–43,48]. We analyze this technique and derive conditions guaranteeing its well-posedness. The extension to systems is then briefly described, underlining the advantage of the $\mathscr{CRD}$ formulation of the linear schemes introduced in the previous section.

5.1. Well-posed nonlinear mappings

Consider the solution of the scalar advection Eq. (20). Given a first-order positive scheme with local residuals $\{\phi_j^{\mathscr{P}}\}_{j\in T}$, we would like to find a set of distribution functions $\{\phi_j\}_{j\in T}$ respecting simultaneously

$$\begin{aligned} &(p)\ \phi_j = \alpha_j \phi_j^{\mathscr{P}}, \alpha_j \geqslant 0 \ \Rightarrow\ \phi_j \phi_j^{\mathscr{P}} \geqslant 0,\\ &(lp)\ \phi_j = \beta_j \phi^h, |\beta_j| < \infty. \end{aligned}$$

Condition (p) guarantees that the resulting scheme is positive, while (lp) ensures linearity preservation. Combining the two and adding the consistency constraint (25), one obtains a scheme for which $\phi_i = 0$ if $\phi^h = 0$ or $\phi_i^{\mathscr{P}} = 0$, otherwise $\phi_i = \beta_i \phi^h$ with

$$\begin{cases} \beta_j \beta_j^{\mathscr{P}} \geqslant 0 \quad \forall j \in T \quad (p),\\ |\beta_j| < \infty \quad \forall j \in T \quad (lp),\\ \sum\limits_{j\in T} \beta_j = 1 \qquad\qquad (c), \end{cases} \tag{78}$$

and

$$\beta_j^{\mathscr{P}} = \frac{\phi_j^{\mathscr{P}}}{\phi^h}. \tag{79}$$

In (78), condition (p) is still dictated by the positivity requirement, condition (lp) guarantees the linearity preservation of the resulting scheme and (c) is the consistency constraint. The goal is then to look for nonlinear mappings

$$\{\beta_j^{\mathscr{P}}\}_{j\in T} \to \{\beta_j\}_{j\in T} \tag{80}$$

preserving the sign of the arguments and guaranteeing the boundedness of the mapped coefficients. Some constructions satisfying (78) can be found in [33,41–43,48]. Most probably the study of these mappings will be the subject of future research. Not surprisingly, the PSI of Struijs [9] belongs to this class of schemes, for a particular choice of the mapping. The results obtained with the schemes generated with this construction, named *limited* or *modified* schemes in [33,41–43,48], are very promising. Nevertheless, as we will show, the applicability of this technique has some limits which have not been underlined. In [42,48] the authors propose to use this construction on higher-order triangular finite elements to obtain nonlinear monotone schemes of accuracy higher than two.

Since on these elements positive first-order $\mathscr{RD}$ schemes do not extend trivially, the authors have used as a basis for the mapping first-order positive schemes on the P1 sub-triangulation (see Fig. 4). In this case, one has

$$\sum_{j\in T} \phi_j^{\mathscr{P}} = \phi^1 \neq \phi^h, \tag{81}$$

since ϕ^h is computed with the higher-order approximation of the unknown, while ϕ^1 is obtained with a piecewise linear approximation. The authors of [42,48] have also remarked that the desired order of accuracy could not be obtained unless the mapping used in the computations was modified to enforce the consistency of the nonlinear scheme. Our objective is to study this case and try to justify the fixes introduced in [42,48] to obtain the desired accuracy. Note that similar ideas have been used also in [34,55] to construct improved and very high-order schemes for time-dependent problems.

To derive conditions for the applicability of the limiting, we analyze the properties verified by the mappings. Consider the case $\phi^h \neq 0$. The consistency constraint (c) in (78) requires that the sum of the bounded nonlinear distribution coefficients must be equal to one. This requires the existence of at least one nonlinear distribution coefficient with positive sign. Because of the positivity condition (p) in (78), this requires the existence of at least one $\beta_j^{\mathscr{P}}$ with positive sign. If the positive first-order scheme is consistent, then

$$\sum_{j\in T} \phi_j^{\mathscr{P}} = \phi^h \quad \text{and} \quad \sum_{j\in T} \beta_j^{\mathscr{P}} = 1. \tag{82}$$

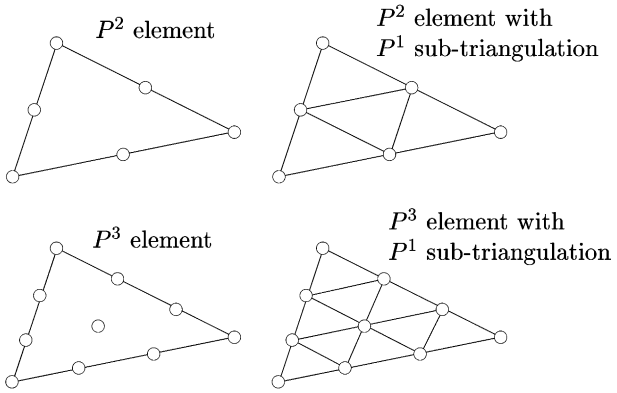

Fig. 4. P^2 and P^3 elements (left) and respective P^1 sub-triangulation (right).

Hence there will be at least one $\beta_j^{\mathscr{P}}$ with positive sign, thus the whole procedure is well defined. More generally, we can say that if $\phi^1\phi^h > 0$, then

$$\sum_{j\in T}\beta_j^{\mathscr{P}} = \sum_{j\in T}\frac{\phi_j^{\mathscr{P}}}{\phi^h} = \frac{\phi^1}{\phi^h} > 0. \tag{83}$$

Hence, there will be at least one $\beta_j^{\mathscr{P}}$ with positive sign and a mapping respecting (78) can be found. As a consequence of this analysis, we can state the necessary condition:

Proposition 1 (Existence of mappings, necessary condition). *A necessary condition to be able to find a construction leading to a mapping (80) satisfying (78) is that*

$$\phi^h\sum_{j\in T}\phi_j^{\mathscr{P}} > 0. \tag{84}$$

Unfortunately, condition (84) is in general almost impossible to ensure and one will encounter the case $\phi^1\phi^h \leqslant 0$. When this happens, the whole construction breaks down, since

$$\sum_{j\in T}\beta_j^{\mathscr{P}} \leqslant 0, \tag{85}$$

and there is no guarantee on the sign of the $\{\beta_j^{\mathscr{P}}\}_{j\in T}$. In particular, when

$$\beta_j^{\mathscr{P}} \leqslant 0 \quad \forall j \in T, \tag{86}$$

the application of the limiting is impossible *unless one relaxes either the positivity (p) or the consistency (c) condition in* (78). Clearly, to the necessary condition (84), we can add the sufficient condition.

Proposition 2 (Well-posedness, sufficient condition). *A sufficient condition for a mapping (80) satisfying (78) to be well-posed is that*

$$\sum_{j\in T}\phi_j^{\mathscr{P}} = \phi^h. \tag{87}$$

We remark that no assumptions have been made on the sign of the nonlinear distribution coefficients. All the mappings proposed in [33,41–43,48] assume $\beta_j \geqslant 0\ \forall j \in T$. This makes our analysis even more important. We are now able to understand why the schemes proposed in [42,48] necessitate a fix to deliver the higher accuracy. Indeed, when $\phi^1 \neq \phi^h$ as in the references, the consistency constraint in (78) is in general not satisfied unless strongly enforced. As a consequence the schemes obtained in this way are inconsistent and hence not convergent [56]. On the other hand, as shown in this section, the consistency condition can be enforced only at the expense of relaxing positivity. Hence, the schemes proposed in [42,48,34,55] are non-positive.

5.2. Nonlinear conservative schemes for conservation laws

The extension of the limiting technique to systems is still a subject of research. For linear symmetric systems, some theoretical results are available in [41–43], where the authors use a wave decomposition technique to reduce the vector of the element residual to a set of scalar residuals. Once the same is done for the local nodal residuals of a first-order monotone matrix scheme, one can apply the limiting on each scalar component. The authors also prove the L_∞-stability of the scheme obtained in this way. The approach has been used to construct linearity preserving and non-oscillatory schemes for the solution of the steady and unsteady Euler equations for a perfect gas in [33,41–43].

Here we use the same procedure. In particular, the numerical results we will present have been obtained by applying the limiting to the linear conservative N1 and N2 schemes introduced in Section 4. Denoting the vector of distributed residuals of the linear schemes by $\{\phi_j^{\mathscr{L}}\}_{j\in T}$, we decompose these vectors in scalar residuals by projecting them on the eigenvectors of

$$K(\bar{\mathbf{u}}) = \frac{\partial \mathscr{F}}{\partial \mathbf{u}} \cdot \vec{u} = R\Lambda L, \tag{88}$$

where $\vec{u}$ denotes the local (model dependent) flow speed. Note that $\vec{u}$, R and L depend on the choice of the local averaged state $\bar{\mathbf{u}}$. If $\{\varphi_j^{\mathscr{L}}\}_{j\in T}$ denote the vectors of scalar (projected) distributed residuals of the linear schemes, and φ^h denotes the vector of the scalar (projected) element residuals, we have

$$\varphi^h = L\phi^h, \quad \varphi_j^{\mathscr{L}} = L\phi_j^{\mathscr{L}} \ \ \forall j \in T. \tag{89}$$

The kth component of $\varphi_i^{\mathscr{L}}$, denoted by $\varphi_{ik}^{\mathscr{L}}$, is then limited. In particular, we set the nonlinear distributed residual φ_{ik} to zero whenever $\varphi_{ik}^{\mathscr{L}} = 0$ or $\varphi_k^h = 0$, otherwise $\varphi_{ik} = \beta_i \varphi_k^h$, where the mapped scalar distribution coefficients are computed as [33,41–43,48]

$$\beta_i = \frac{\max(0, \beta_i^{\mathscr{L}})}{\sum_{j\in T} \max(0, \beta_j^{\mathscr{L}})}, \quad \beta_j^{\mathscr{L}} = \frac{\varphi_{jk}^{\mathscr{L}}}{\varphi_k^h}. \tag{90}$$

The residuals are then transformed back to conservative variables:

$$\phi_j = R\varphi_j \quad \forall j \in T. \tag{91}$$

We refer to the resulting schemes as to the nonlinear LN1 and LN2 scheme. Note that, due to the $\mathscr{CRD}$ formulation, the sufficient condition of Proposition 2 is met *by construction* by the linear schemes, that is, we always have

$$\sum_{j\in T} \varphi_{jk}^{\mathscr{L}} = \varphi_k^h. \tag{92}$$

Hence, the additional advantage of the conservative formulation proposed in this paper is that it allows to construct linear schemes always guaranteeing the well-posedness of the limiting. Hence, the LN1 and LN2 schemes are always well defined. They are linearity preserving by construction and conservative independently on the degree of nonlinearity of the fluxes $\mathscr{F}(\mathbf{u})$, due to the definition (71) of the residual. Their robustness and non-oscillatory character will be extensively proved by the numerical tests presented in the next sections.

6. Computational details and numerical results

This section is devoted to the discussion of the numerical results obtained with the linear conservative N1 and N2 schemes and their limited variants, the nonlinear LN1 and LN2 schemes. Before discussing the results we summarize the solution procedure and give some details relative to the practical implementation of the schemes. Then we present the results obtained by solving the Euler equations for a perfect gas. Even if in this case a conservative linearization does exist [1], the results show that with our formulation one can use other linearizations. This simplifies the definition of the schemes while guaranteeing the preservation of the non-oscillatory character of the results. Finally we show the application to a system lacking a conservative linearization for which the use of our approach is essential to guarantee conservation.

6.1. Implementation details

Starting from $\mathbf{u}^n = \mathbf{u}^h(x,y,t = t^n)$, we march in time as follows:

1. *Time-step computation.* The time step Δt is computed according to
$$\Delta t = 0.75 \min_{T\in\tau_h} \Delta t_T \tag{93}$$
with Δt_T given by (61). The eigenvalues needed in (61) are computed using the arithmetic average of $\{\mathbf{u}_j^n\}_{j\in T}$ to linearize the jacobians. Clearly (93) is a very strict time-step constraint. We remark once more that it can be overcome by using the two-layer formulation of [28–30]. This aspect is however out of the scopes of this paper which focuses on the conservation and shock-capturing properties of the linear and nonlinear schemes proposed. Similarly, we observe that the time-step constraint for the positivity of the N2 scheme (Eq. (54) in the linear case) would allow to use a larger time step which would probably lead to slightly better (less diffusive) results with this scheme, due to the reduced number of iterations. The time-step restriction for the positivity of the LN2 scheme is however obtained by the *local* positivity analysis of the N2 scheme. As shown in [33,34], this condition turns out to be precisely (61).
2. *Space–time residual.* For all T the space–time residual (71) is computed. Consistently with the choice of linear variation of $\mathbf{u}^h$ in space, the line integrals of the flux $\mathscr{F}(\mathbf{u}^h)$ are approximated with a 2 points Gaussian formula (see [57] for a study on the influence of the number of Gauss' points in flux quadrature). Note, however, that improvements can be made in this respect. As shown in [15], second order of accuracy only requires the approximation of the boundary integral of the flux to be $\mathscr{O}(h^3)$. This is already obtained with a linear interpolation of $\mathscr{F}$ in space, that is, using trapezium rule on each edge. As the choice of the time-stepping strategy, the choice of the flux quadrature is an important aspect with respect to the efficiency of the schemes and certainly needs further refinement.
3. *Residual distribution.* The residual is distributed to the nodes of T. For the linear N1 and linear N2 schemes we use Eqs. (74) and (76) respectively. The average state $\bar{\mathbf{u}}$ is given by the arithmetic average of $\{\mathbf{u}_j^{n+1}\}_{j\in T}$ in the case of the N1 scheme. For the N2 scheme we use the average of $\{\mathbf{u}_j^n\}_{j\in T}$ in (77) and in the corresponding part of the residual and the average of $\{\mathbf{u}_j^{n+1}\}_{j\in T}$ to compute $\mathbf{u}_c^{n+1}$ and in the corresponding part of the residual. To obtain the nonlinear LN1 and LN2 schemes, we apply the limiting of Section 5. The wave decomposition (88) is performed by taking $\bar{\mathbf{u}}$ as the average of $\{\mathbf{u}_j^{n+1}\}_{j\in T}$ and the scalar distribution coefficient are computed according to (90). We recall that the well-posedness of the limiting is guaranteed by the consistency of the linear schemes. Conservation is guaranteed by the boundary integration of the fluxes.
4. *Solve nonlinear system.* A nonlinear algebraic system formally identical to (42) is solved. As in [28–30,35,44] we use an explicit pseudo-time iterative procedure. For the linear schemes, a few explicit iterations are enough to converge the L_1 norm of the nodal residuals four or five orders of magnitude in pseudo-time and a number of iterations from 20 to 40 are necessary to converge to machine accuracy. As in [33], convergence to machine accuracy is never obtained with the nonlinear schemes. A number of explicit iterations of the order of 20–40 is needed for a residual drop of three or four order of magnitude in pseudo-time. We remark that this *does not* pose any problems with respect to grid convergence, as a consequence of the fact that ϕ^h in (71) is of $\mathscr{O}(h^3, \Delta t^2)$ and of the residual character of the schemes. As confirmed by the numerical experience, when reducing the mesh size h, *any* norm of the nodal residual of the nonlinear schemes converges to values increasingly close to machine zero in the inner pseudo-time iterations. This guarantees that the error due to the poor convergence is always within the truncation error. Concerning the choice of the explicit iterative procedure, we mention that in [58,59] the authors have compared the explicit pseudo-time stepping approach to an implicit Newton algorithm for the solution of the nonlinear algebraic system arising from the space–time $\mathscr{RD}$ discretization of the Euler and

Navier–Stokes equations obtained with the schemes of [28–30]. For inviscid problems containing strong discontinuities, like the ones considered here, the explicit method results in a faster convergence in terms of CPU time.

Steps 1–4 are repeated until $t^{n+1} = t^n + \Delta t = t_f$.

6.2. Numerical results: Euler equations for a perfect gas

The Euler equations for a perfect gas can be written as in (1) with

$$\mathbf{u} = \begin{pmatrix} \rho \\ \rho u \\ \rho v \\ \rho E \end{pmatrix}, \quad \mathscr{F} = \begin{pmatrix} \rho u & \rho v \\ \rho u^2 + p & \rho uv \\ \rho uv & \rho v^2 + p \\ \rho uH & \rho vH \end{pmatrix},$$

where ρ is the fluid density, $\vec{u} = (u, v)$ is the velocity vector, p is the thermodynamic pressure, while E and H are the total specific energy and enthalpy, respectively. The system is closed by the relations:

$$H = E + p/\rho, \quad p = (\gamma - 1)\rho\left(E - \frac{\vec{u}\cdot\vec{u}}{2}\right),$$

where γ the ratio of the specific heats, assumed to be equal to 1.4.

6.3. Moving shocks

To asses to shock capturing capabilities of the schemes we performed computations of moving planar shocks. We discretize the spatial domain $[0, 2] \times [0, 0.1]$ using two different meshes: an unstructured one containing 2166 nodes and 3910 triangles ($h \approx 1/100$) and a structured one composed of quads ($h = 1/100$) cut into triangles using the right running diagonals (see Fig. 5). Periodic boundary conditions in the y direction are imposed. The initial solution is an exact Mach 10 moving shock located at $x = 0.5$. The final time has been set to $t_f = 0.1$, corresponding to a displacement of the shock of a length $L_x = 1$. No relevant differences have been observed between the results obtained on the two different meshes. In Figs. 6 and 7 we show the pressure and density profiles obtained on the unstructured grid. We plot the data

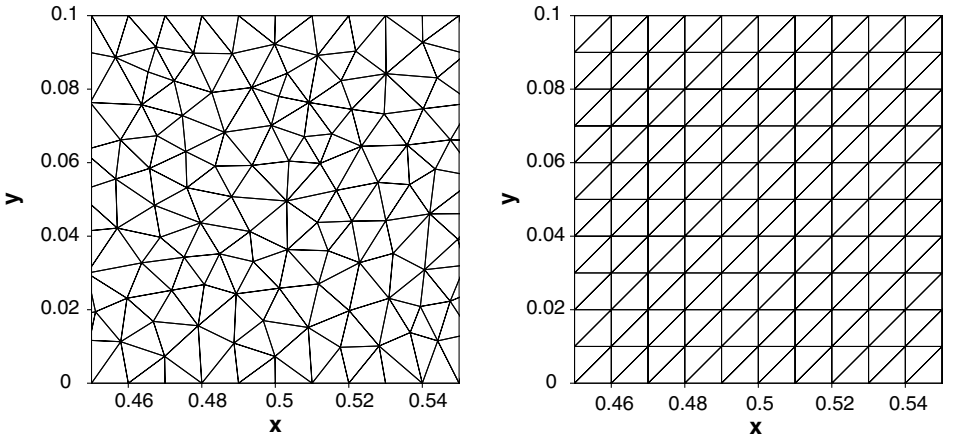

Fig. 5. Unstructured (left) and structured (right) triangulation.

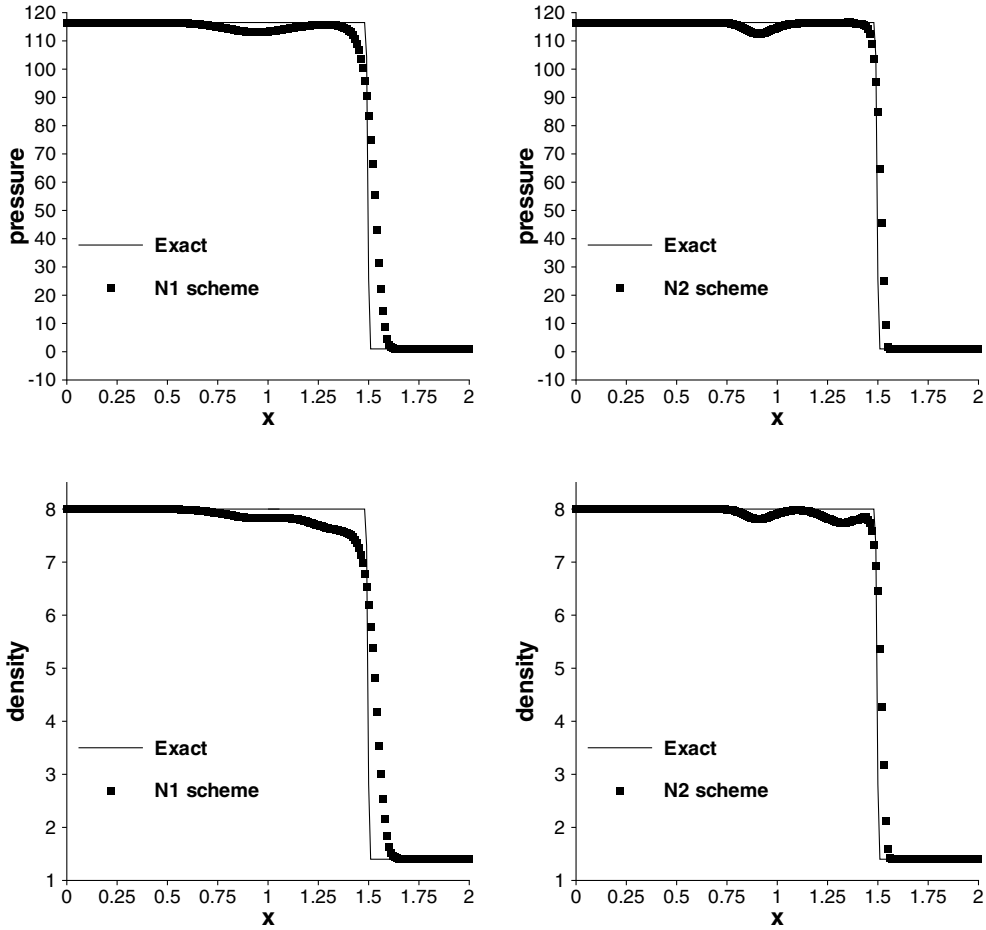

Fig. 6. Mach 10 moving shock. Pressure (top row) and density (bottom row) profiles at time $t = 0.1$. 201 points extracted at $y = 0.05$. N1 scheme (left column) and N2 scheme (right column).

obtained extracting 201 points on the line $y = 0.05$. The shock position is computed correctly by all the schemes, indicating their conservative nature. The results of the limited schemes (Fig. 7) show indeed a sharper capturing of the discontinuity. In all the density profiles, we can see two perturbations moving upstream of the shock. Only one of them is present in the pressure distributions. We claim that these perturbations are due to a discretization error at $t = 0$. To confirm this hypothesis we have run the simulations on finer meshes. The results are summarized in Fig. 8. On the left in the figure we report the results obtained on structured triangulations with the linear N2 scheme. We show the nodal values of the density in the middle of the domain for mesh sizes $h = 1/100$ and $h = 1/500$. We see that as the mesh is refined, a reduction of the error is indeed observed. However, due to the fact that the error is generated in correspondence of the initial singularity, this reduction is of less than $\mathcal{O}(h)$. The scheme splits the error in components moving along the characteristic directions. It can be easily checked that the perturbation closer to the origin of the x-axis moves with speed $u_L - a_L$, being a_L the speed of sound after the shock. We conclude that this must be the projection of the error generated at $t = 0$ on the characteristic corresponding to the *slow acoustic* speed. Similarly, the second perturbation moves with speed u_L and hence it is the projection of the error on the

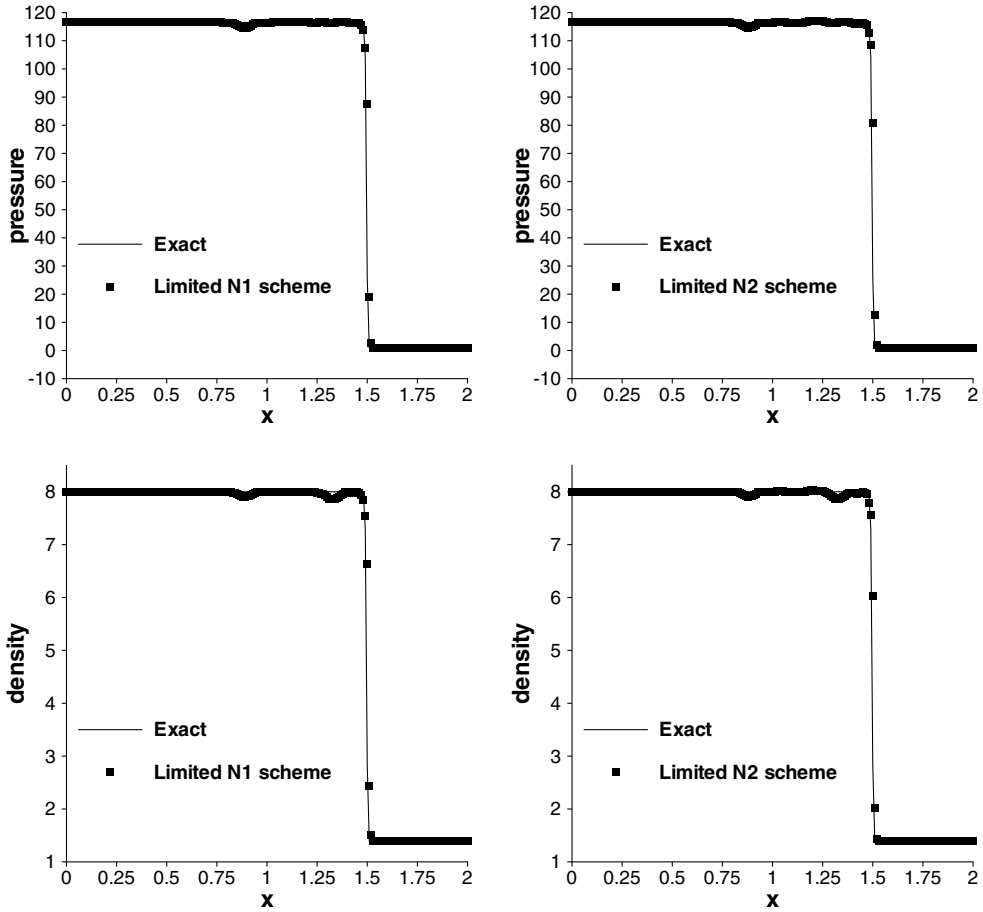

Fig. 7. Mach 10 moving shock. Pressure (top row) and density (bottom row) profiles at time $t = 0.1$. 201 points extracted at $y = 0.05$. nonlinear LN1 scheme (left column) and LN2 scheme (right column).

entropy field, as confirmed by its absence in the pressure distributions. Probably a third component of the error, which we have been unable to detect, is also present. Similar conclusions can be drawn from the right picture in Fig. 8 where the results obtained with the LN2 scheme on the regular mesh with $h = 1/500$ are reported. Comparing this result with the one on Fig. 7, we see again that the reduction of the error is indeed small.[2] Analog results have been obtained with the linear N1 and the nonlinear LN1 scheme. These effects, however, are not induced by the conservative approach we propose. We performed the same computations using the $\mathscr{LRD}$ N2 scheme of [33,43] obtaining results identical to the ones given by the $\mathscr{CRD}$ variant proposed here. A similar behavior is observed also for the space–time schemes of [28–30]. We attribute the appearance of this error to the difference between the exact jump relations and their piecewise linear approximation on the mesh actually seen by the schemes. This difference produces the small amplitude perturbations seen in the results when applying the schemes to the initial *exact* shock. However, other explanations could be possible [60,61] and this behavior certainly deserves a more detailed study. It must be

[2] The error on the finer mesh is about half of the error on the coarse one.

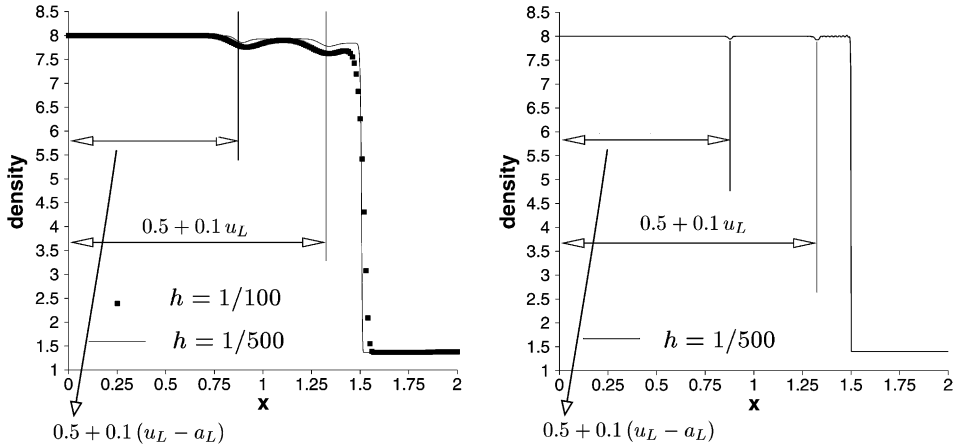

Fig. 8. Mach 10 shock: error propagation. N2 (left) and LN2 (right) scheme.

noted anyway that, apart from these perturbations, the nonlinear schemes produce a very sharp and monotone capturing of the discontinuity.

6.4. A 2D Riemann problem

This problem is taken from [33]. At time $t = 0$ the velocity is set to zero, and the following discontinuity in pressure and density is imposed:

$$p = \begin{cases} 1 & \text{if } xy \geqslant 0, \\ 0.1 & \text{otherwise,} \end{cases} \qquad \rho = \begin{cases} 1 & \text{if } xy \geqslant 0, \\ 0.1 & \text{otherwise.} \end{cases}$$

We compute the solution up to time $t = 0.2$ on an unstructured discretization of the spatial domain $[-1, 1]^2$ containing 39,822 nodes and 78,842 triangles, with $h \approx 1/100$ as in [33]. Contour plots of the computed density field are given in Fig. 9, while a comparison of the numerical solutions on the lower boundary of the domain with the exact one-dimensional solution of the problem is reported in Fig. 10. All the discontinuities are computed monotonically, with the proper strength and in the correct positions as it can be clearly seen in Fig. 10. From the plots, one notes a striking difference between the results given by the linear N1 scheme and the nonlinear LN1 scheme. Similarly, a remarkable difference is observed between the solutions of the linear N1 and N2 scheme. Of all the schemes, the N1 yields the worst results in terms of accuracy. As already remarked in Section 3, this is a direct consequence of the extra numerical dissipation introduced by the upwinding in space–time. However, the results of the LN1 and LN2 schemes are nearly identical: both produce a very crisp resolution of the wave interactions and a non-oscillatory approximation of the discontinuities. This is very interesting since it suggests that, as far as the nonlinear scheme is linearity preserving, the results are qualitatively almost independent on the nature of the underlying linear scheme. Note that the quality of our results is comparable to the one achieved in [33].

6.5. Double Mach reflection on a ramp

This is a severe test for the robustness and the accuracy of schemes designed to compute discontinuous flows containing complex structures. It consists of the interaction of a planar Mach 10 shock with a 30° ramp. See [62] for a detailed description. The simulation has been run on an unstructured triangulation

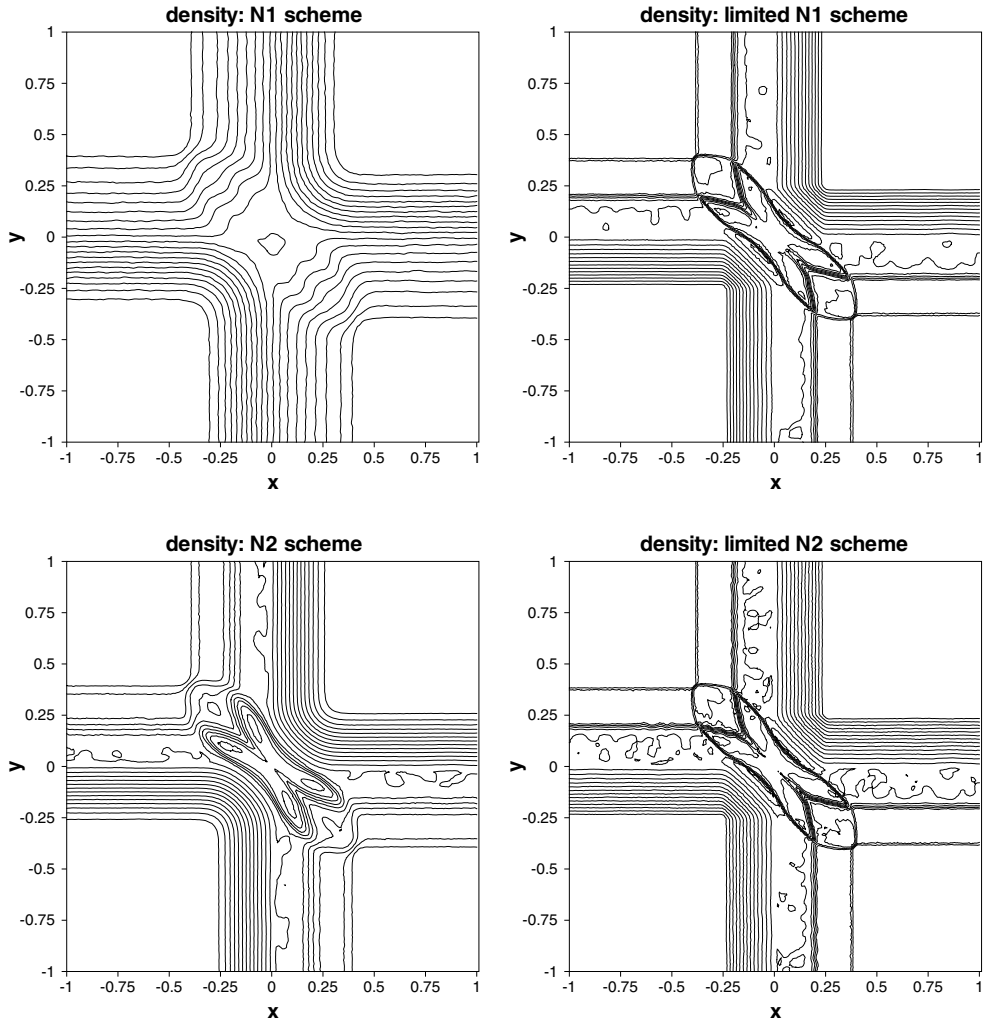

Fig. 9. 2D Riemann problem. Density contours at time $t = 0.2$. Top: N1 (left) and LN1 scheme (right); Bottom: N2 (left) and LN2 scheme (right).

(see Fig. 5) with $h \approx 1/100$. We use a rotated frame of reference, with the x-axis aligned with the ramp [62]. As it is customary for this test, we plot the contours of the density field. In Fig. 11 three results are shown. On the top we report the solution obtained with a second-order cell-centered $\mathscr{FV}$ scheme using Roe's numerical flux, linear reconstruction and limiter proposed in [63] and a second-order Runge–Kutta time integrator. On the middle and bottom pictures, we show the results obtained (on the same mesh) with the nonlinear LN1 and LN2 scheme respectively. All the schemes resolve quite well the interaction between the shock and the ramp. However, the resolution of the contact emanating from the triple point and of the jet of fluid on the wall improves going from the top to the bottom picture, the $\mathscr{FV}$ scheme giving the worst result. The two limited $\mathscr{RD}$ schemes show a sharper capturing of these features and of the shock. For this test, the nonlinear LN2 scheme gives the best result.

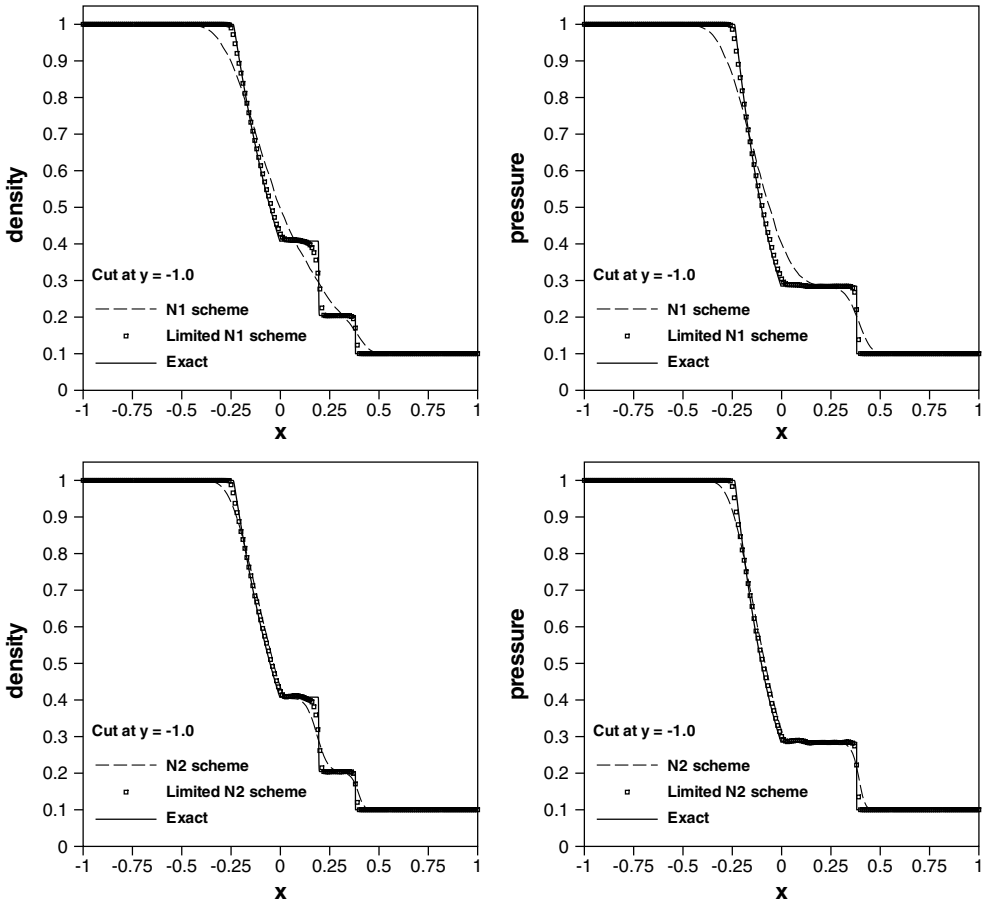

Fig. 10. 2D Riemann problem. Density (left) and pressure (right) at $t = 0.2$ and $y = -1.0$. Top: N1 and LN1 schemes; Bottom: N2 and LN2 schemes.

6.6. A shock–shock interaction

This test has been included to assess the shock-capturing capabilities of the schemes in a true multidimensional situation. It is one of the two-dimensional Riemann problems studied in [64] and later used also in [65,26,24]. The problem consists of the interaction of two oblique shocks with two normal shocks. All the discontinuities are moving backwards with respect to the speed in the pre-shock region as depicted in the sketch on the left in Fig. 12. With reference to the notation of the figure, the initial data are given by

$$(\rho, u, v, p) = \begin{cases} (1.5, 0, 0, 1.5) & \text{state } a, \\ (0.1379928, 1.2060454, 1.2060454, 0.0290323) & \text{state } b, \\ (0.5322581, 1.2060454, 0, 0.3) & \text{state } c, \\ (0.5322581, 0, 1.2060454, 0.3) & \text{state } d. \end{cases}$$

The computations have been run on an unstructured discretization of the spatial domain $[0, 1] \times [0, 1]$ with reference mesh size $h = 1/200$. A zoom of the grid in vicinity of the diagonal is shown on the right in Fig. 12. We compare the numerical solution obtained with the LN2 scheme with the one of the $\mathscr{FV}$ scheme used in

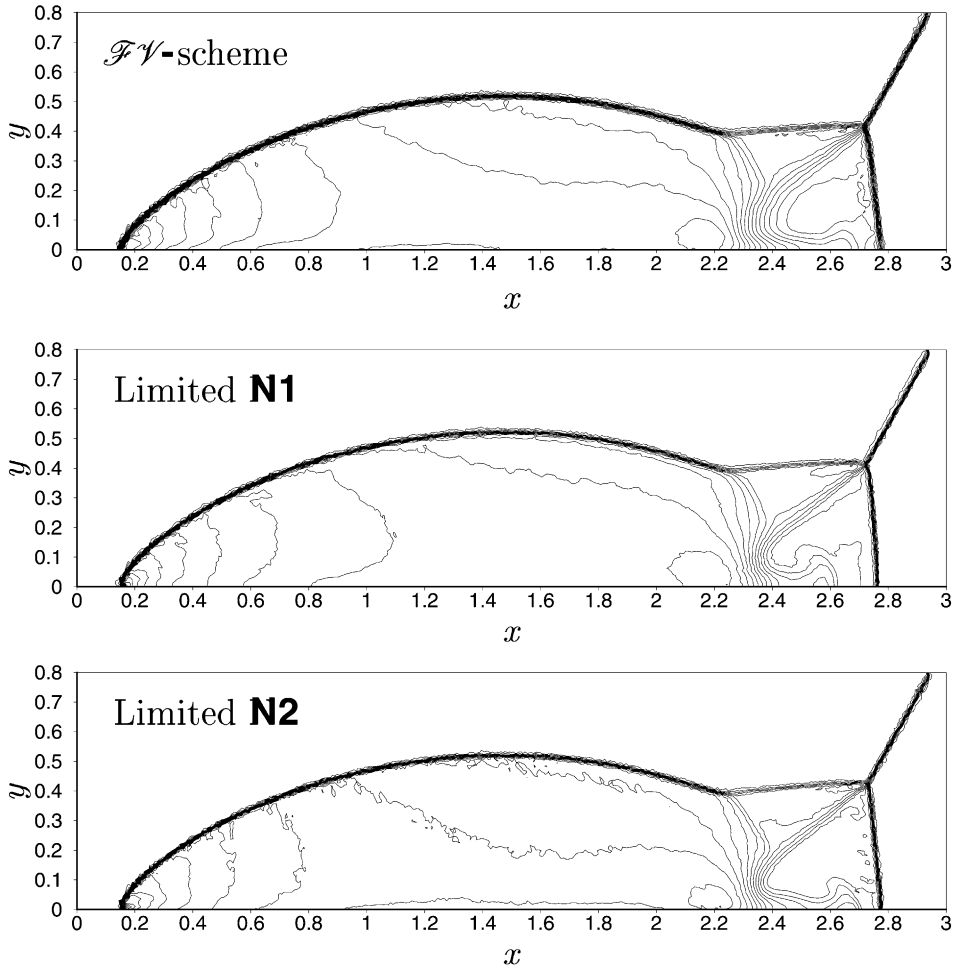

Fig. 11. Double Mach reflection. Density at time $t = 0.2$. Cell-centered $\mathscr{FV}$ scheme (top), LN1 scheme (middle) and LN2 scheme (bottom).

the double Mach reflection test. As in [65,26,24] we compute the interaction up to time $t = 0.8$ and visualize the results in terms of contours of the density (Fig. 13). We also report, in Fig. 14, the distributions of density and pressure along the diagonal (symbols *do not* correspond to mesh points). The plots in Fig. 13 show that both schemes capture the complex structures in the solution: the interaction of the shocks generates two symmetric lambda-shaped couples of shocks and a downward moving normal shock; very strong slip lines emanate from the lower triple points and interact with one of the branches of the upper lambda shocks, while a jet of fluid is pushed from the high pressure region (state a) against the normal shock. Despite of the irregularity of the grid, both schemes yield quite monotone and accurate results. However, the LN2 scheme gives a much richer solution. The region of the jet is better resolved and so are the contact lines showing, already on this mesh resolution, the onset of Kelvin–Helmoltz instabilities. The distributions of pressure and densities along the diagonal confirm the superiority of the $\mathscr{RD}$ scheme as well as its monotone character. The reader is referred to [34] for similar results obtained with the limited $\mathscr{LRD}$ N2 scheme on finer meshes and to [26,24] for results obtained with a different nonlinear $\mathscr{RD}$ scheme on structured triangular meshes.

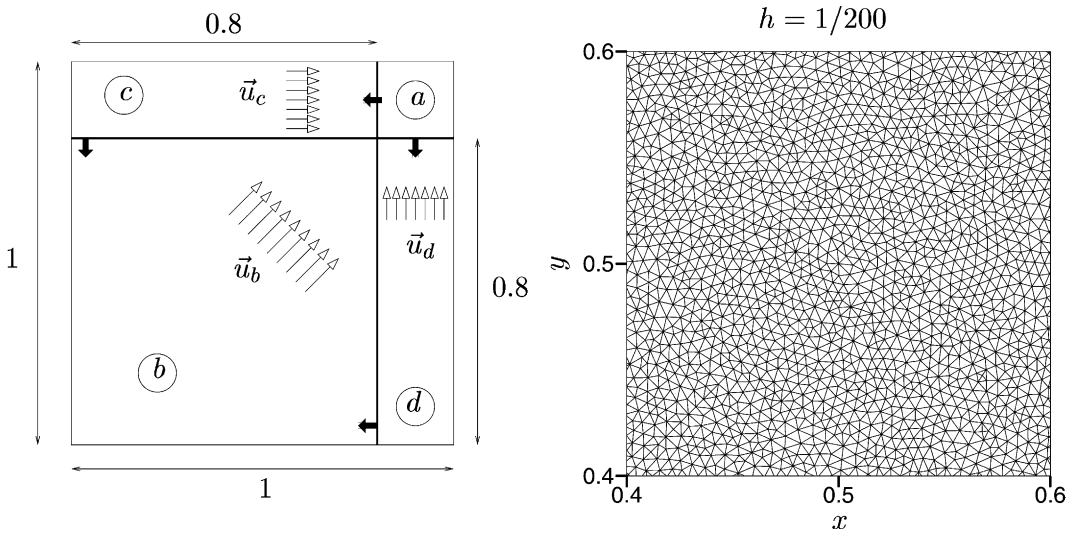

Fig. 12. Shock–shock interaction. Initial solution (left) and zoom of the grid (right).

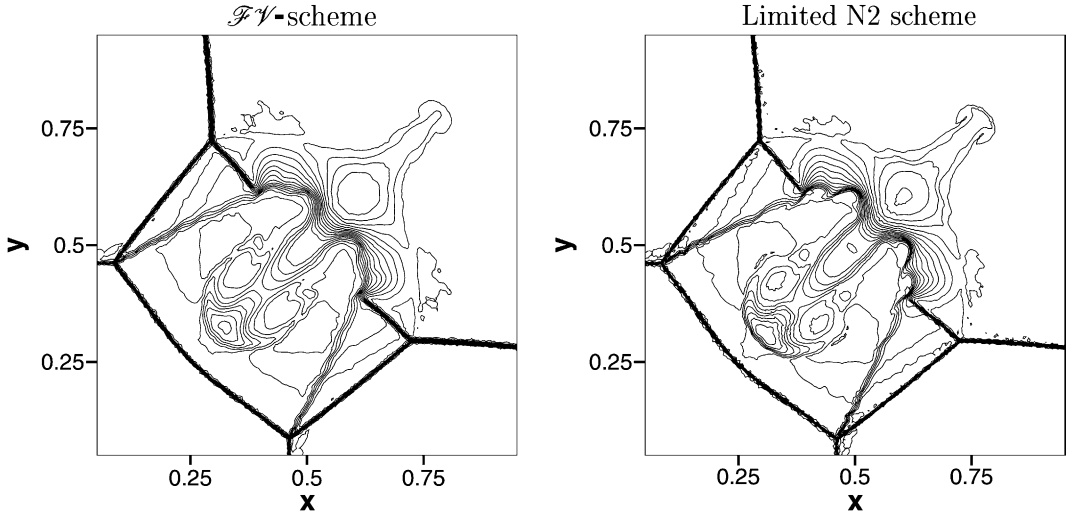

Fig. 13. Shock–shock interaction. Contours of the density obtained with: $\mathscr{FV}$ scheme (left) and LN2 scheme (right).

6.7. Numerical results: homogeneous two-phase flow

In this section, we consider the hyperbolic system given by (1) with

$$\mathbf{u} = \begin{pmatrix} \alpha_g \rho_g \\ \alpha_l \rho_l \\ \rho u \\ \rho v \end{pmatrix}, \quad \mathscr{F} = \begin{pmatrix} \alpha_g \rho_g u & \alpha_g \rho_g v \\ \alpha_l \rho_l u & \alpha_l \rho_l v \\ \rho u^2 + p & \rho uv \\ \rho uv & \rho v^2 + p \end{pmatrix},$$

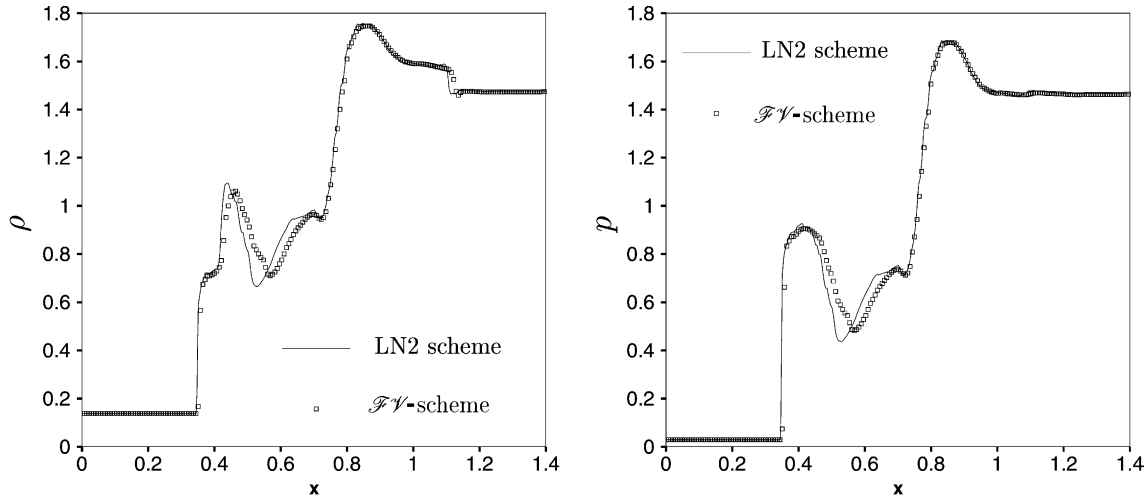

Fig. 14. Shock–shock interaction. Density (left) and pressure (right) distribution along the symmetry line. $\mathcal{FV}$ scheme (symbols) and LN2 scheme (line).

where α_g and α_l are gas and liquid *volume fractions*, ρ_g and ρ_l are gas and liquid densities, p is the pressure, $\vec{u} = (u, v)$ is the velocity vector and ρ is the mixture density defined by

$$\rho = \alpha_g \rho_g + \alpha_l \rho_l. \tag{94}$$

The phasic volume fractions respect the constraint

$$\alpha_g + \alpha_l = 1. \tag{95}$$

Due to (95), we will denote simply by α, the gas volume fraction α_g, often referred to as the *void fraction*. The system is closed by the equations of state. In this work, we have used the following relations [66]:

$$p = \Gamma_g \left(\frac{\rho_g}{\rho_{g0}} \right)^{\gamma_g} \tag{96}$$

with $\Gamma_g = 10^5$ Pa, $\rho_{g0} = 1$ kg/m^3, $\gamma_g = 1.4$, and

$$p = \Gamma_l \left[\left(\frac{\rho_l}{\rho_{l0}} \right)^{\gamma_l} - 1 \right] + p_{l0} \tag{97}$$

with $\Gamma_l = 3.31 \times 10^8$ Pa, $\rho_{l0} = 1000$ kg/m^3, $\gamma_l = 7.15$, $p_{l0} = 10^5$ Pa. This system of equations constitutes a fairly simple model of homogeneous air–water two-phase flow [66]. It has however some appealing features for the purpose of testing our schemes. The first one is exactly its simplicity, while the second being the fact that it is fully hyperbolic and its complete eigenstructure can be analytically derived. Most importantly, the model is in strong conservation law form and one can compute exact steady and unsteady Rankine–Hugoniot relations against which to test the schemes. However, the relation between the pressure and the conserved mass and momentum fluxes is so complex that a conservative linearization can hardly be derived. Moreover, because of the nonlinearity of the equations of state, pressure and volume fractions cannot be computed in closed form from the conserved variables. Instead, combining the equations of state and relation (95), a nonlinear equation for the pressure is obtained which can be solved in a few Newton iterations (see [66] for more).

6.8. Moving shocks in air–water mixtures

To further confirm the conservative character of our schemes, we present computations of a planar shock moving in a quiescent two-phase mixture containing 50% gas and 50% liquid ($\alpha_{lR} = \alpha_{gR} = \alpha_R = 0.5$) at a pressure $p_R = 10^6$ Pa. To define the strength of the shock, we use the Mach number

$$M_S = \frac{u_S}{\sqrt{p_R/\rho_R}},$$

where u_S is the velocity of the shock and ρ_R is the density of the undisturbed mixture. Here we consider the case $M_S = 3$. The spatial domain is the rectangle $[0, 2] \times [0, 0.1]$. The simulations have been run on the meshes of Fig. 5 with periodic boundary conditions in the y direction. The final time of the simulation t_f has been fixed to $1/u_S$, corresponding to a displacement of the exact shock of a length $L_x = 1$. At time $t = 0$ the shock is located at $x = 0.5$ m. No visible differences have been observed between the solutions obtained on the unstructured and on the structured triangulation and only the results obtained on the

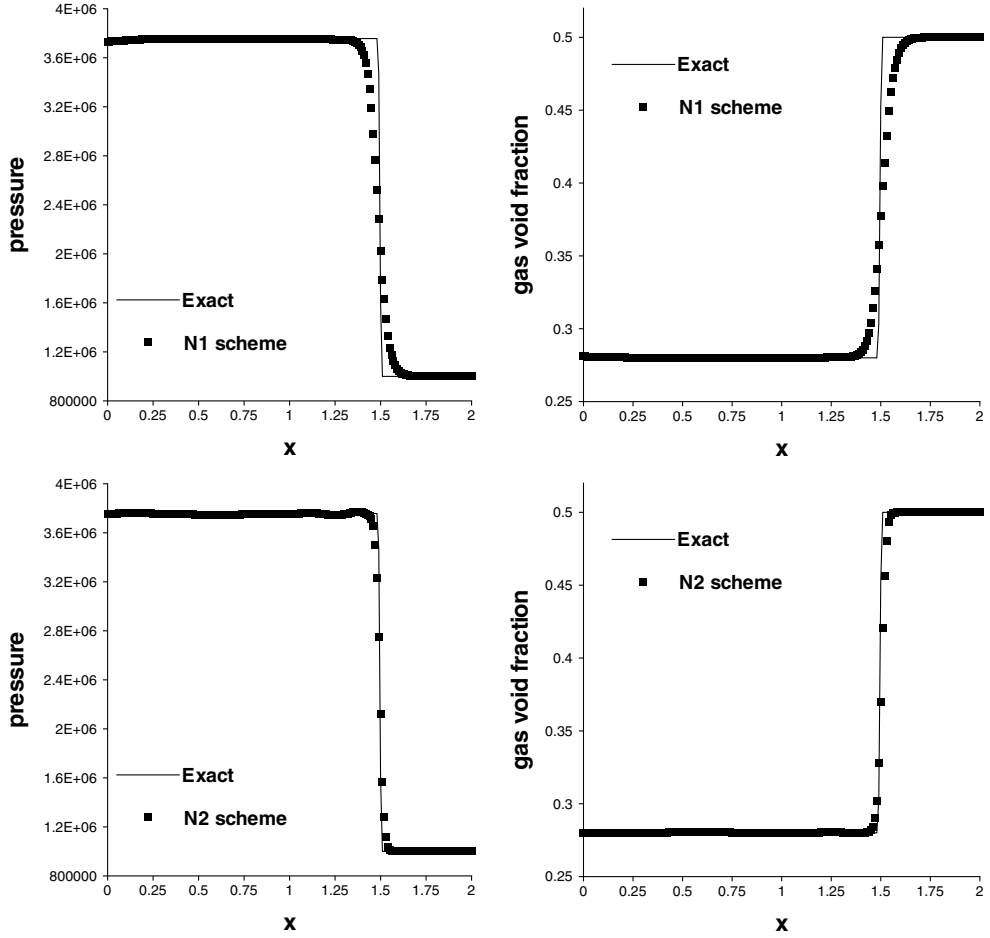

Fig. 15. $M_S = 3$ moving shock. Pressure (left column) and gas void fraction (right column). 1D cut at $y = 0.05$ (201 points). N1 (top) and N2 (bottom) schemes.

unstructured grid are reported. The plots on Figs. 15 and 16 show pressure and gas void fraction distributions obtained by extracting 201 points along the line $y = 0.05$. The shock position is correctly computed. The non-oscillatory character of the results is also clear from the figures. The perturbations seen in the case of the Euler equations are not visible, probably due to the weaker character of this shock. The nonlinear schemes give a very sharp and monotone capturing of the discontinuity.

6.9. A two-phase 2D Riemann problem

This problem is meant to be an analog of the two-dimensional Riemann problem of Section 6.2. The initial solution is given by a still mixture with $\alpha = 0.5$ in which the following discontinuity in the pressure is imposed:

$$p = \begin{cases} 10^7 \text{ Pa} & \text{if } xy \geqslant 0, \\ 10^8 \text{ Pa} & \text{otherwise.} \end{cases}$$

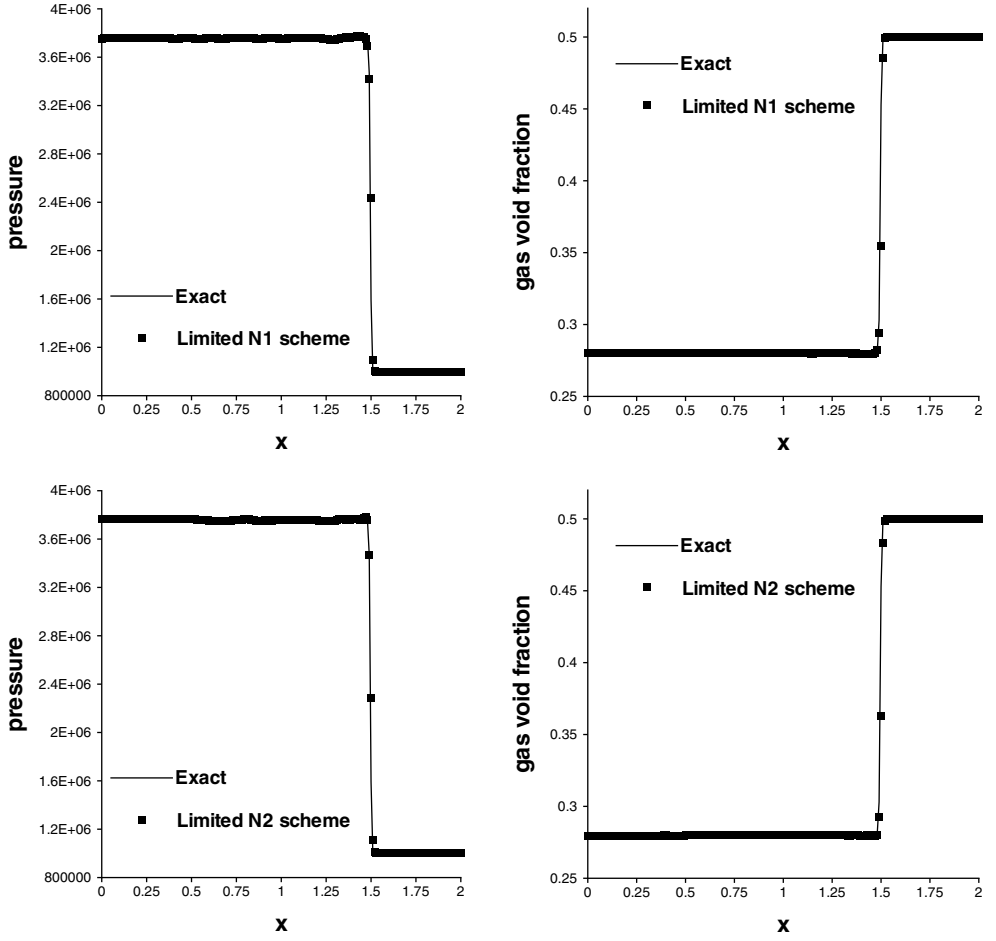

Fig. 16. $M_S = 3$ moving shock. Pressure (left) and gas void fraction (right). 1D cut at $y = 0.05$ (201 points). LN1 (top) and LN2 (bottom) schemes.

The problem is solved on the domain $[-5, 5]^2$ up to time $t = 0.004$ s on an unstructured mesh containing 19,932 triangles and 10,167 nodes ($h = 1/10$). In Fig. 17 we show the contours of the mixture density (94) for all the schemes. On the boundaries of the domain three distinct waves are visible: an expansion, a contact and a shock. Both the shock and the contact are noticeably better computed by the nonlinear schemes. Moving away from the boundaries, we see how the waves interact with each other. The higher resolution of the limited schemes is visible also from the fact that the lines of constant density in the expansion are kept straight for a longer distance from the boundary. As in the case of the Euler equations, there is a remarkable difference between the results of the linear N1 scheme and of the linear N2 scheme. The latter gives a visibly better resolution of the discontinuities. Nevertheless, also for this problem we see that the nonlinear LN1 and LN2 schemes yield nearly identical results. In Fig. 18, we compare the solutions along the top boundary of the domain with a reference solution, given is in this case by a numerical solution

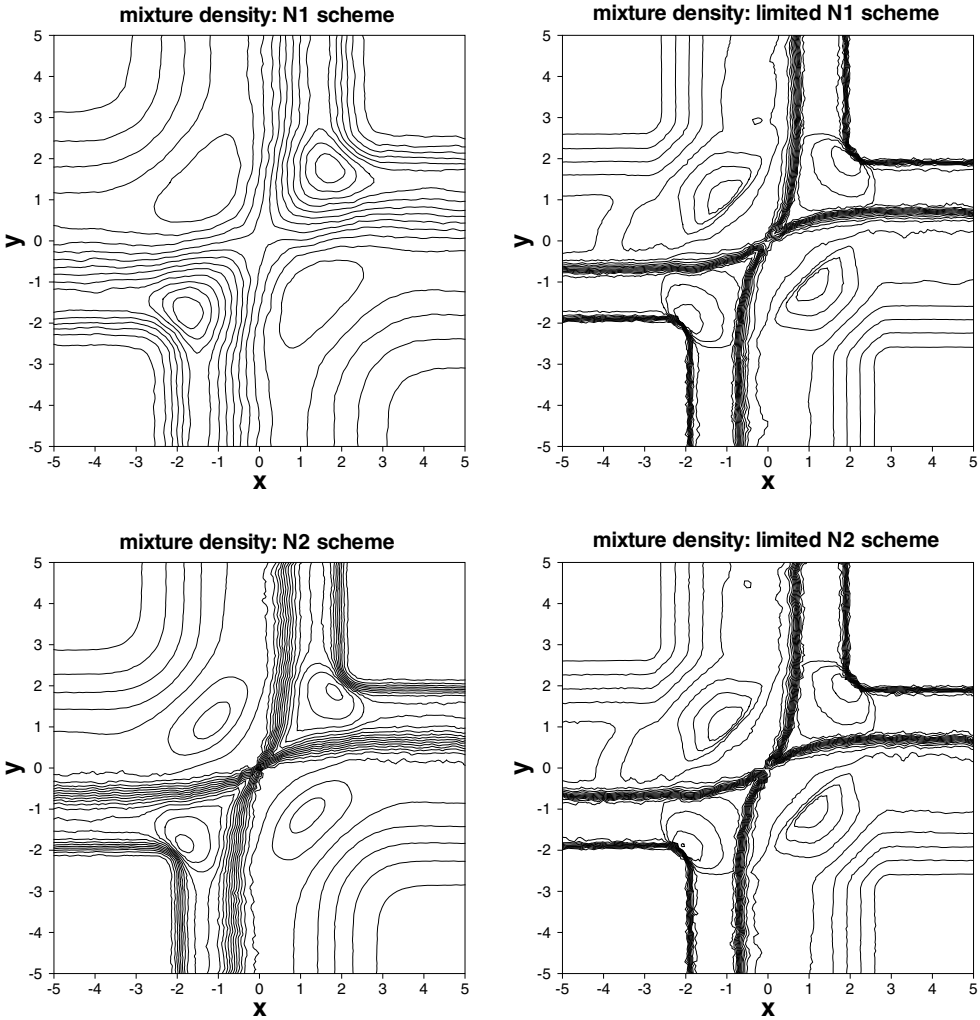

Fig. 17. 2D two-phase Riemann problem. Mixture density contours at time $t = 0.004$. Top: N1 (left) and LN1 scheme (right); Bottom: N2 (left) and LN2 scheme (right).

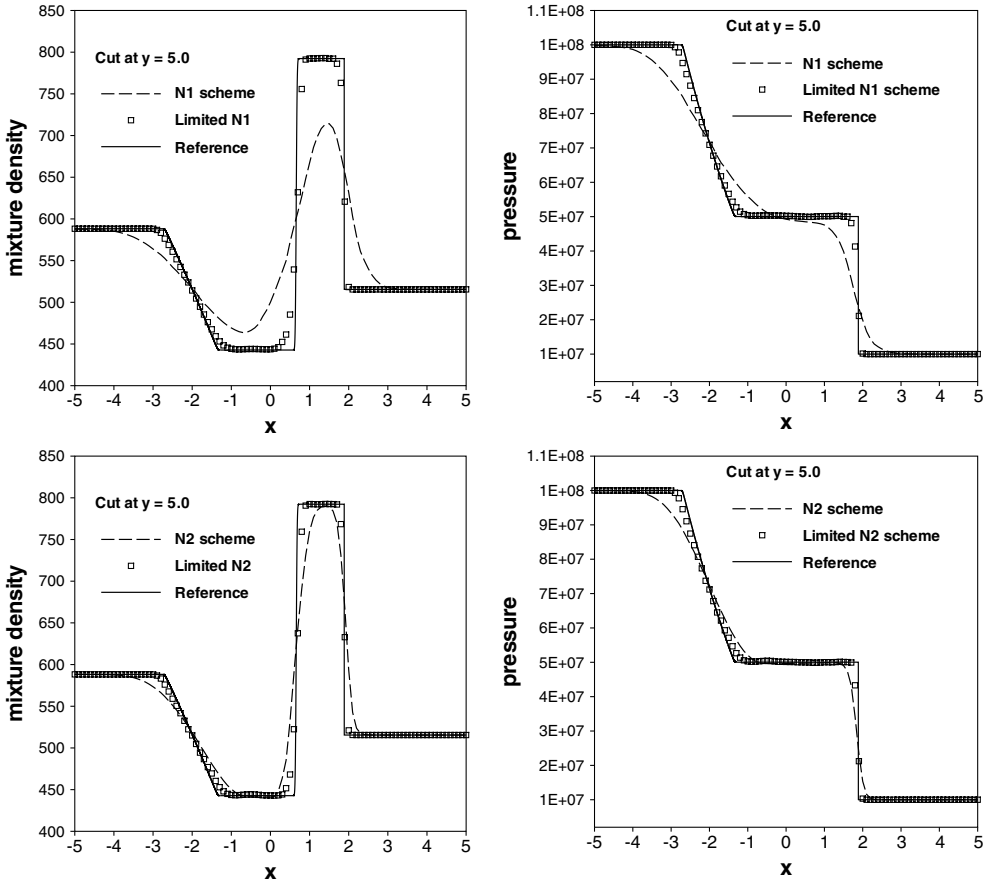

Fig. 18. 2D two-phase Riemann problem. Mixture density (left) and pressure (right) distribution at time $t = 0.004$ and $y = 5.0$. Top: N1 and LN1 scheme against reference; Bottom: N2 and LN2 scheme against reference.

obtained on a very fine one-dimensional mesh containing 50,000 cells with the first-order conservative finite volume scheme of [67]. All the schemes reproduce correctly positions and strength of the shocks. The capturing of all the discontinuities is monotone and very sharp in the case of the two limited schemes.

6.10. A two-phase shock–bubble interaction

The last test presented in the paper is a two-phase *shock–bubble* interaction. The initial solution (sketched in Fig. 19) consists of a planar shock with $M_S = 3$ moving into an undisturbed quiescent mixture characterized by $\alpha_R = 0.8$ and $p_R = 10^5$ Pa. On the right of the shock, a circular discontinuity in which the void fraction jumps to $\alpha = 0.95$ is present. The discontinuity is centered at $x = 0.3$ and $y = 0$ and its radius is $r_b = 0.2$ m. For symmetry reasons, only half of the interaction has been computed. A zoom of the grid used for the computations is shown in Fig. 19. The mesh size is $h \approx 1/200$. The results are visualized in terms of contours of the mixture density (94) in Fig. 20. Note that in each picture, we have plotted the solution obtained with the nonlinear LN1 scheme on the top half and the one obtained with the nonlinear LN2 scheme on the bottom half. From the figures we see the shock partially transmitted through the void fraction discontinuity and partially reflected as an expansion, while the contact itself is set into motion. Once the shock

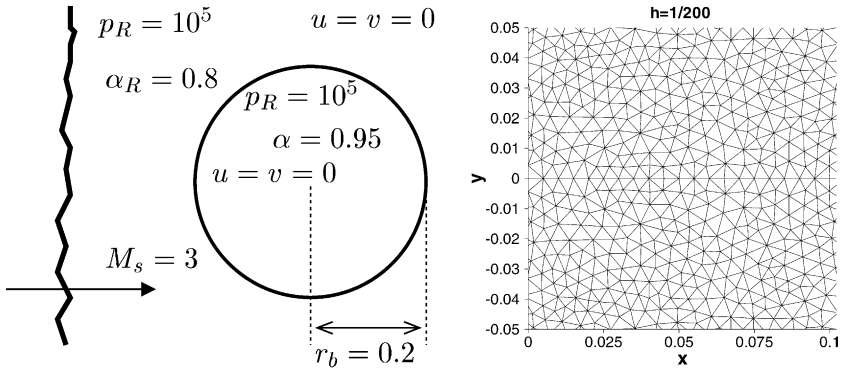

Fig. 19. Two-phase shock–bubble interaction. Mesh (left) and initial solution (right).

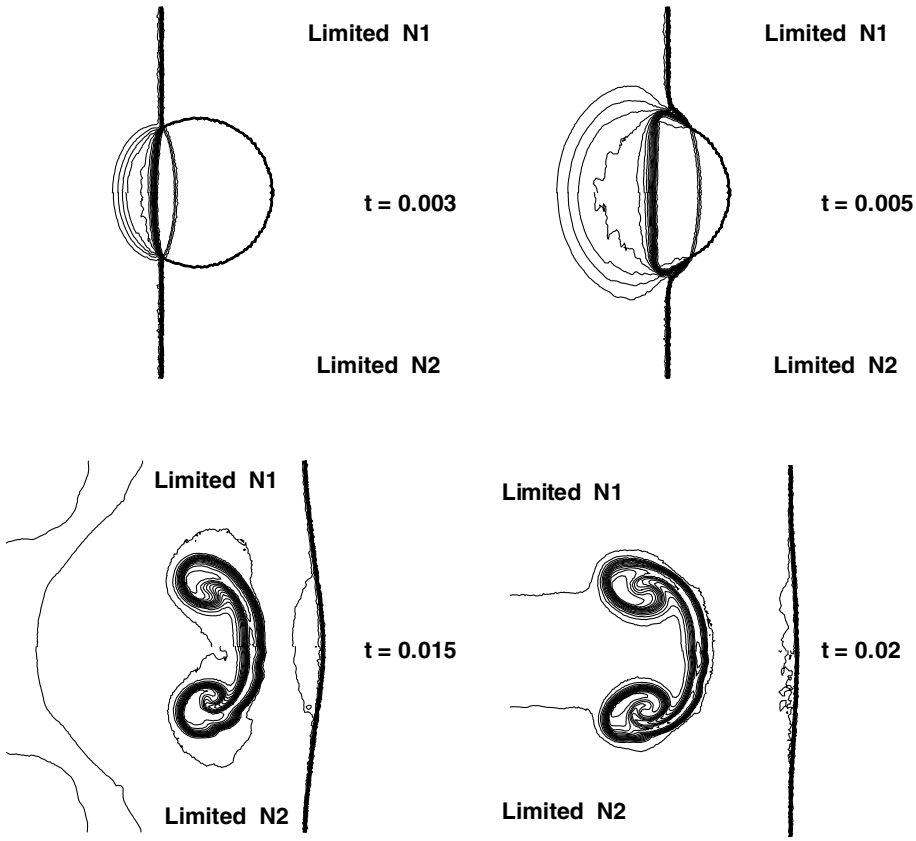

Fig. 20. Two-phase shock–bubble interaction. Mixture density contours at different times. In each figure, on top results obtained with the nonlinear LN1 scheme and on the bottom results obtained with the nonlinear LN2 scheme.

has traversed the whole circular discontinuity and joined the transmitted shock, the interface of the contact folds, rolling-up into a symmetric structure. Also in this computation the LN2 scheme shows a smaller numerical dissipation. Indeed, it gives a crisper resolution of the contact, its wavy structure (bottom pictures) even giving the glimpse of an inviscid instability. The results of the LN1 scheme, however, are not

extremely more dissipative, the scheme still providing a sharp resolution of this complex interaction. These results compare qualitatively well to the ones presented in [68,69] for the Euler equation for a perfect gas and to the ones obtained with different two-phase flow models and numerics in [70–72]. We remark however that our objective is not the simulation of two-phase flow per se. The development of numerical methods for two-phase flow simulations represents in itself a whole research field. The contribution of this paper is to provide a formulation of Residual Distribution schemes that can be used in this field.

7. Conclusions

In this paper we propose a conservative space–time formulation of residual distribution schemes for the approximation of unsteady weak solutions of general hyperbolic systems of conservation laws. In particular, we show how to construct nonlinear linearity preserving conservative schemes yielding a stable, sharp and non-oscillatory approximation of strong interacting discontinuities. These schemes are very competitive with the state of the art $\mathscr{FV}$ schemes [63] in terms of accuracy and resolution of complex flow features but use a more compact stencil of nearest neighbors only. To construct these schemes, two independent issues have been studied. The first is the definition of conservative schemes for time-dependent systems of conservation laws lacking a Roe linearization. This problem has been solved extending the $\mathscr{CRD}$ formulation of residual distribution [44] to the space–time framework. Linear first-order non-oscillatory schemes have been obtained by constructing conservative $\mathscr{CRD}$ variants of the linear N1 and N2 matrix schemes proposed in [35] and [32,33] respectively. The $\mathscr{CRD}$ N1 and N2 schemes have been numerically shown to yield a non-oscillatory approximation of discontinuous solutions of conservation laws even in presence of complex thermodynamics. Starting from these linear schemes we constructed nonlinear linearity preserving conservative schemes. We have presented an analysis of the nonlinear limiting strategy proposed in [33,41–43,48] and we have formulated conditions for its well-posedness, showing the need of consistent linear monotone schemes for the discretization of multidimensional conservation laws. Combining the space–time $\mathscr{CRD}$ formulation with the limiting technique, we obtained nonlinear high-order and non-oscillatory schemes for the solution of general time-dependent conservation laws. The consistency of the linear $\mathscr{CRD}$ schemes always guarantees the well-posedness of the nonlinear mapping. The nonlinear LN1 and LN2 schemes obtained in this way have been extensively tested on problems involving the propagation and the interaction of strong discontinuities. Both schemes have shown promising features: conservation, generality, sharp and monotone capturing of complex flow structures.

The approach we propose gives a solid basis for the use of $\mathscr{RD}$ schemes for the solution of very general systems of equations. Application is under way to the Euler equations for gases in thermochemical equilibrium, to the shallow-water equations, and to more general two-phase flow models. Even though in [44], the application of the $\mathscr{CRD}$ approach to the solution of the ideal MHD equations in conservative form has been already shown, improved conservative formulations are being developed. However, some issues still remain open. The first is related to efficiency. For practical computations, the two-layer variant of the schemes will allow the use of higher values of the time step Δt. In our experiments, we have seen that the results obtained with the two-layer schemes are practically identical to the ones obtained with the schemes described in the paper. Similarly, a considerable reduction of the computational cost could be obtained by properly assessing the influence of the choice of the flux quadrature formulas used to compute the residual. However, some more basic efficiency issues are present. Among these we mention the following. The N scheme at the basis of all our constructions is very expensive, due to the need of inverting numerically small full matrices in every element. Moreover, it shows stability and accuracy problems in the low speed and transonic cases, due to the presence of vanishing eigenvalues of the flux jacobians and of the wrong scaling of the numerical dissipation in the low Mach regime. This is not surprising, the scheme being a multidimensional generalization of Roe's flux difference splitter [1,53,73]. The low Mach accuracy and

stability problems can be cured by the use of preconditioning techniques [10]. For all the singularities of the scheme, not shared by the space–time variants proposed in [28–30,35], fixes can be designed [74,14,15,75]. Even so, the computational cost of the scheme remains. As seen in Sections 6.2 and 6.7, even if the linear N1 scheme shows a greater numerical dissipation compared to the linear N2 scheme, the differences between the nonlinear LN1 and LN2 schemes are not as important as for the linear schemes. This suggests that simpler schemes could be used as a basis for the limiting. Even if the N scheme is the least dissipative linear first-order scheme, at the level of the limited schemes the differences in the results could be negligible. For instance, one could choose a linear positive scheme which makes the minimum use of the quasi-linear form of the equations, thus avoiding most of the problems arising from the singularities of the flux Jacobians. The $\mathscr{RD}$ formulation of the Lax-Friederichs scheme studied in [41–43] is a good example of such a scheme. This will certainly involve a more detailed study of the mappings used in the limiting. Concerning the application to the computations of *real-life* flows, a very important issue to investigate is the behavior of the schemes in presence of very strong contact discontinuities. In [44], it has been shown that, provided that the pressure is used as a primary unknown, steady contacts can be resolved exactly if aligned with the mesh. A more general investigation of this topic is needed, on the lines of the work done in [70,76]. Similarly, a deeper investigation of the structure of the numerical shock profiles would be interesting, perhaps following the ideas in [60,61]. Analytical studies on regular grids could help to make a link to previous results obtained in the context of Finite Volume discretizations.

Acknowledgments

The authors gratefully acknowledge Remi Abgrall for the many discussions and remarks on the construction of nonlinear $\mathscr{RD}$ and on the approximation of flows containing strong contact discontinuities. Jiří Dobeš is also acknowledged for running the Finite Volume computations.

References

[1] H. Deconinck, P.L. Roe, R. Struijs, A multidimensional generalization of Roe's difference splitter for the Euler equations, Comput. Fluids 22 (2/3) (1993) 215–222.
[2] H. Paillère, H. Deconinck, Compact cell vertex convection schemes on unstructured meshes, in: H. Deconinck, B. Koren (Eds.), Euler and Navier–Stokes Solvers Using Multi-Dimensional Upwind Schemes and Multigrid Acceleration, Notes on Numerical Fluid Mechanics, vol. 57, Vieweg, Braunschweig, 1997, pp. 1–49.
[3] H. Paillère, H. Deconinck, Multidimensional upwind residual distribution schemes for the 2D Euler equations, in: H. Deconinck, B. Koren (Eds.), Euler and Navier–Stokes Solvers Using Multi-Dimensional Upwind Schemes and Multigrid Acceleration, Notes on Numerical Fluid Mechanics, vol. 57, Vieweg, Braunschweig, 1997, pp. 51–112.
[4] A. Bonfiglioli, H. Deconinck, Multidimensional upwind schemes for the 3D Euler equations on unstructured tetrahedral meshes, in: H. Deconinck, B. Koren (Eds.), Euler and Navier–Stokes Solvers Using Multi-Dimensional Upwind Schemes and Multigrid Acceleration, Notes on Numerical Fluid Mechanics, vol. 57, Vieweg, Braunschweig, 1997, pp. 141–185.
[5] E. van der Weide, H. Deconinck, Matrix distribution schemes for the system of Euler equations, in: H. Deconinck, B. Koren (Eds.), Euler and Navier–Stokes Solvers Using Multi-Dimensional Upwind Schemes and Multigrid Acceleration, Notes on Numerical Fluid Mechanics, vol. 57, Vieweg, Braunschweig, 1997, pp. 113–139.
[6] E. van der Weide, H. Deconinck, E. Issmann, G. Degrez, Fluctuation splitting schemes for multidimensional convection problems: an alternative to finite volume and finite element methods, Comput. Mech. 23 (2) (1999) 199–208.
[7] H. Deconinck, G. Degrez, Multidimensional Upwind Residual Distribution Schemes and Applications. Finite Volumes for Complex Applications II, Hermes Science Publications, Paris, 1999.
[8] H. Deconinck, K. Sermeus, R. Abgrall, Status of multidimensional upwind residual distribution schemes and applications in aeronautics, AIAA paper 2000-2328, AIAA CFD Conference, Denver, USA, June 2000.
[9] R. Struijs, A multi-dimensional upwind discretization method for the Euler equations on unstructured grids, PhD thesis, University of Delft, Netherlands, 1994.

[10] H. Paillère, Multidimensional upwind residual discretization schemes for the Euler and Navier–Stokes equations on unstructured meshes, PhD thesis, Université Libre de Bruxelles, 1995.
[11] E. Issman, G. Degrez, H. Deconinck, Implicit upwind residual-distribution Euler and Navier–Stokes solver on unstructured meshes, AIAA J. 34 (1996) 2021–2028.
[12] E. van der Weide, H. Deconinck, Positive matrix distribution schemes for hyperbolic systems, in: Computational Fluid Dynamics, Wiley, New York, 1996, pp. 747–753.
[13] E. van der Weide, Compressible flow simulation on unstructured grids using multi-dimensional upwind schemes, PhD thesis, Delft University of Technology, Netherlands, 1998.
[14] K. Sermeus, H. Deconinck, Solution of the steady Euler and Navier–Stokes equations using residual distribution schemes, VKI LS 2003-05, 33rd Computational Fluid dynamics Course, von Karman Institute for Fluid Dynamics, 2003.
[15] R. Abgrall, Toward the ultimate conservative scheme: following the quest, Comput. J. Phys. 167 (2) (2001) 277–315.
[16] J. Maerz, G. Degrez, Improving time accuracy of residual distribution schemes, Technical Report VKI-PR 96-17, von Karman Institute for Fluid Dynamics, 1996.
[17] A. Ferrante, H. Deconinck, Solution of the unsteady Euler equations using residual distribution and flux corrected transport, Technical Report VKI-PR 97-08, von Karman Institute for Fluid Dynamics, 1997.
[18] D. Caraeni, S. Conway, L. Fuchs, About a Parallel Multidimensional Solver for LES. Finite Volumes for Complex Applications II, Hermes Science Publications, Paris, 1999.
[19] D. Caraeni, L. Fuchs. LES using a parallel multidimensional upwind solver, in: ICCFD, First International Conference on Computational Fluid Dynamics, Kyoto, Japan, July 2000.
[20] D. Caraeni, L. Fuchs, A new compact high-order multidimensional upwind discretization, in: 4th World CSCC Conferene, Vouliagmeni, Greece, July 2000.
[21] D. Caraeni, M. Caraeni, L. Fuchs, A paralles multidimensional upwind algorithm for LES, in: 15th AIAA Computational Fluid Dynamics Conference, Anaheim, CA, USA, June 2001.
[22] D. Caraeni, L. Fuchs, Compact third-order multidimensional upwind scheme for Navier–Stokes simulations, Theor. Comput. Fluid Dynamics 15 (2002) 373–401.
[23] D.A. Caraeni, Development of a multidimensional upwind residual distribution solver for large eddy simulation of industrial turbulent flows, PhD thesis, Lund Institute of Technology, 2000.
[24] P. De Palma, G. Pascazio, G. Rossiello, M. Napolitano, Accurate solutions to unsteady problems by monotone implicit fluctuation splitting schemes, in: 16th AIAA Computational Fluid Dynamics Conference, Orlando, FL, USA, June 2003.
[25] M. Hubbard, P.L. Roe, Compact high resolution algorithms for time dependent advection problems on unstructured grids, Int. J. Numer. Methods Fluids 33 (5) (2000) 711–736.
[26] P. De Palma, G. Pascazio, M. Napolitano, An accurate fluctuation splitting scheme for the unsteady two-dimensional Euler equations, in: ECCOMAS CFD Conference, Swansea, Wales, UK, September 2001.
[27] M. Ricchiuto, H. Deconinck, Time-accurate solution of hypercolic partial differential equations using FCT and residual distribution, Technical Report VKI-SR 99-33, von Karman Institute for Fluid Dynamics, 1999.
[28] Á. Csík, H. Deconinck, Space–time residual distribution schemes for hyperbolic conservation laws on unstructured linear finite elements, in: M.J. Baines (Ed.), ICFD Conference on Numerical Methods for Fluid Dynamics VII, Oxford, 2001, pp. 557–564.
[29] Á. Csík, M. Ricchiuto, H. Deconinck, S. Poedts, Space–time residual distribution schemes for hyperbolic conservation laws, in: 15th AIAA Computational Fluid Dynamics Conference, Anaheim, CA, USA, June 2001.
[30] Á. Csík, H. Deconinck, Space time residual distribution schemes for hyperbolic conservation laws on unstructured linear finite elements, Int. J. Numer. Methods Fluids 40 (2002) 573–581.
[31] R. Abgrall, M. Mezine. A consistent upwind residual scheme for scalar unsteady advection problems, in: Conference AMIF 2000, organized by the European Science Foundation, Tuscany, Italy, October 2000.
[32] M. Mezine, R. Abgrall, Upwind multidimensional residual schemes for steady and unsteady flows, in: ICCFD2 International Conference on Computational Fluid Dynamics 2, Sidney, Australia, July 2002, pp. 165–170.
[33] R. Abgrall, M. Mezine, Construction of second order accurate monotone and stable residual distribution schemes for unsteady flow problems, J. Comput. Phys. 188 (2003) 16–55.
[34] M. Mezine, M. Ricchiuto, R. Abgrall, H. Deconinck, Monotone and stable residual distribution schemes on prismatic space–time elements for unsteady conservation laws, VKI LS 2003-05, 33rd Computational Fluid dynamics Course, von Karman Institute for Fluid Dynamics, 2003.
[35] Á. Csík, M. Ricchiuto, H. Deconinck, Space–time residual distribution schemes for hyperbolic conservation laws over linear and bilinear elements, VKI LS 2003-05, 33rd Computational Fluid dynamics Course, von Karman Institute for Fluid Dynamics, 2003.
[36] P.L. Roe. Linear advection schemes on triangular meshes, Technical Report CoA 8720, Cranfield Institute of Technology, 1987.
[37] P.L. Roe. "Optimum" upwind advection on a triangular mesh, Technical Report, ICASE, NASA Langley R.C., 1990.
[38] M.E. Hubbard, M.J. Baines, Conservative multidimensional upwinding for the steady two-dimensional shallow-water equations, J. Comput. Phys. 138 (1997) 419–448.

[39] Á. Csík, H. Deconinck, S. Poedts, Monotone residual distribution schemes for the ideal magnetohydrodynamic equations on unstructured grids, AIAA J. 39 (8) (2001) 1532–1541.
[40] R. Abgrall, T.J. Barth, Residual distribution schemes for conservation laws via adaptive quadrature, SIAM J. Sci. Comput. 24 (3) (2002) 732–769.
[41] R. Abgrall, M. Mezine, Construction of second-order accurate monotone and stable residual distribution schemes for steady flow problems, J. Comput. Phys. 195 (2004) 474–507.
[42] R. Abgrall, M. Mezine, Residual distribution schemes for steady problems, VKI LS 2003-05, 33rd Computational Fluid dynamics Course, von Karman Institute for Fluid Dynamics, 2003.
[43] M. Mezine, Conception de Schémas Distributifs pour l'aérodynamique stationnaire et instationnaire, PhD thesis, École doctorale de mathmatiques et informatique, Université de Bordeaux I, 2002.
[44] Á. Csík, M. Ricchiuto, H. Deconinck, A conservative formulation of the multidimensional upwind residual distribution schemes for general nonlinear conservation laws, J. Comput. Phys. 179 (2) (2002) 286–312.
[45] T. Quintino, M. Ricchiuto, Á. Csík, H. Deconinck, Conservative multidimensional upwind residual distribution schemes for arbitrary finite elements, in: ICCFD2 International Conference on Computational Fluid Dynamics 2, Sidney, Australia, July 2002.
[46] P. De Palma, G. Pascazio, D.T. Rubino, M. Napolitano, Multidimensional upwind cell-vertex schemes for quadrilaterals, in: ECCOMAS CFD Conference 2004, Jyväskyl, July 2004.
[47] S.T. Zalesak, Fully multidimensional flux-corrected transport algorithms for fluids, J. Comput. Phys. 31 (1979) 335–362.
[48] R. Abgrall, P.L. Roe, High order fluctuation schemes on triangular meshes, SIAM J. Sci. Comput. 19 (3) (2003) 3–36.
[49] T.J. Barth, Numerical methods for conservation laws on structured and unstructured meshes, VKI LS 2003-05, 33rd Computational Fluid dynamics Course, von Karman Institute for Fluid Dynamics, 2003.
[50] S.K. Godunov, A finite difference method for the numerical computation of discontinuous solutions of the equations of fluid dynamics, Mat. Sb. 47 (1959).
[51] Á. Csík, Upwind residual distribution schemes for general hyperbolic conservation laws and application to ideal magnetohydrodynamics, PhD thesis, Katholieke Universiteit Leuven, Faculteit Wetenschappen Centrum voor Plasma-Astrofysica, Belgium, 2002.
[52] C. Bolley, M. Crouzeix, Conservation de la positivité lors de la discétization des problèmes d'èvolution paraboliques, R.A.I.R.O. Analyse Numèrique 12 (1978) 237–254.
[53] P.L. Roe, Approximate Riemann solvers, parameter vectors, and difference schemes, J. Comput. Phys. 43 (1981) 357–372.
[54] P.L. Roe, D. Sidilikover, Optimum positive linear schemes for advection in two and three dimensions, SIAM J. Numer. Anal. 29 (6) (1992) 1542–1568.
[55] M. Ricchiuto, R. Abgrall, H. Deconinck, Construction of very high order residual distribution schemes for unsteady advection: preliminary results, VKI LS 2003-05, 33rd Computational Fluid dynamics Course, von Karman Institute for Fluid Dynamics, 2003.
[56] R. Abgrall, K. Mer, B. Nkonga, A Lax–Wendroff type theorem for residual schemes, in: M. Haffez, J.J. Chattot (Eds.), Innovative Methods for Numerical Solutions of Partial Differential Equations, World Scientific, 2002, pp. 243–266.
[57] T.J. Barth,P.O. Frederickson, High order solution of the Euler equations on unstructured grids using quadratic reconstruction, AIAA paper 90-0013, 28th AIAA Aerospace Sciences Meeting, Reno, NV, USA, January 1990.
[58] J. Dobeš, M. Ricchiuto, H. Deconinck, Implicit space–time residual distribution method for unsteady viscous flow, in: 16th AIAA Computational Fluid Dynamics Conference, Orlando, FL, USA, June 2003.
[59] J. Dobeš, M. Ricchiuto, H. Deconinck, Implicit space–time residual distribution method for unsteady laminar viscous flow, Comput. Fluids 34 (4) (2005) 593–619.
[60] M. Arora, P.L. Roe, On post-shock oscillations due to shock capturing schemes in unsteady flows, J. Comput. Phys. 130 (1997) 25–40.
[61] S. Jin, J.-G. Lin, The effects of numerical viscosities – I. Slowly moving shocks, J. Comput. Phys. 126 (1996) 373–389.
[62] P.R. Woodward, P. Colella, The numerical simulation of two-dimensional flows with strong shocks, J. Comput. Phys. 54 (1984) 115–173.
[63] T.J. Barth, D.C. Jespersen, The design and application of upwind schemes on unstructured meshes, AIAA paper 89-0355, 27th AIAA Aerospace Sciences Meeting, Reno, NV, USA, January 1989.
[64] A. Kurganov, E. Tadmor, Solution of two-dimensional Riemann problems without Riemann solvers, Numer. Methods Partial Differential Equations 18 (2002) 548–608.
[65] R.J. LeVeque, Wave propagation algorithms for multi-dimensional hyperbolic systems, J. Comput. Phys. 131 (1997) 327–353.
[66] H. Paillère, C. Corre, J. Garcia, On the extension of the AUSM + scheme to compressible two-fluid models, Comput. Fluids 32 (6) (2003) 891–916.
[67] L.C. Huang, Pseudo-unsteady difference schemes for discontinuous solutions of steady-state one dimensional fluid dynamics problems, J. Comput. Phys. 42 (1981) 195–211.
[68] H. Holden, K.-A. Lie, N.H. Risebro, An unconditionally stable method for the Euler equations, J. Comput. Phys. 150 (1999) 76–96.

[69] J.O. Langseth, R.J. LeVeque, A wave propagation method for three-dimensional hyperbolic conservation laws, J. Comput. Phys. 165 (2000) 126–166.
[70] R. Abgrall, B. Nkonga, R. Saurel, Efficient numerical approximation of compressible multi-material flow for unstructured meshes, Comput. Fluids 32 (2003) 571–605.
[71] R.P. Fedkiw, T. Aslam, B. Mettiman, S. Osher, A non-oscillatory eulerian approach to interfaces in multimaterial flows (the ghost fluid method), J. Comput. Phys. 152 (1999) 457–492.
[72] R.K.S. Hankin, The Euler equations for multiphase compressible flow in conservation form – simulation of shock–bubble interactions, J. Comput. Phys. 172 (2001) 808–826.
[73] M. Ricchiuto, D.T. Rubino, J.A.S. Witteveen, H. Deconinck, A residual distributive approach for one-dimensional two-fluid models and its relation with Godunov finite volume schemes, in: Proceedings of the International Workshop on Advanced Numerical Methods for Multidimensional Simulation of Two-Phase Flow, Garching, Germany, 2003.
[74] K. Sermeus, H. Deconinck, An entropy fix for multidimensional upwind residual distribution schemes, Comput. Fluids 34 (4) (2005) 617–640.
[75] K. Sermeus, H. Deconinck, An entropy fix for the multidimensional upwind residual distribution schemes, in: CFD2002, 10th Annual Conference of the CFD Society of Canada, Windsor, Ont., Canada, June 9–11, 2002.
[76] R. Abgrall, How to prevent pressure oscillations in multicomponent flows: a quasi-conservative approach, J. Comput. Phys. 125 (1) (1996) 150–160.